Aspects of Molecular Medicine 5 (2025) 100086

Contents lists available at ScienceDirect

Aspects of Molecular Medicine

journal homepage: www.journals.elsevier.com/aspects-of-molecular-medicine

In-silico identification of phytochemicals as potential therapeutic agents to inhibit the HMG-CoA reductase activity using computational approach

Sheetal Dagar [a], Anil Panwar [a,*], Dushyant Gahalyan [a], Neeru Redhu [a], Mukesh Kumar [b], Sunil Kumar [c], Varruchi Sharma [d], Heera Ram [e], Ravikant Verma [f], Anil Sharma [g]

[a] *Department of Bioinformatics and Computational Biology, CCS Haryana Agricultural University, Hisar, 125004, India*
[b] *Department of Biotechnology, Ambala College of Engineering and Applied Research Mithapur, Ambala, Haryana, 133101, India*
[c] *Department of Botany, CRM Jat College, Hisar, 125001, India*
[d] *Department of Biotechnology, Sri Guru Gobind Singh College, Chandigarh, 160001, India*
[e] *Department of Zoology, Jai NarainVyasUniversity, Jodhpur, 342001, India*
[f] *Department of Zoology, CCS Haryana Agricultural University, Hisar, 125004, India*
[g] *Department of Biotechnology, Amity University, Mohali, 140306, India*

A R T I C L E I N F O

Handling Editor: Prof A Angelo Azzi

Keywords:
ADMET
Phytochemicals
HMG-CO A reductase
molecular docking
MDsimulation
MM-P/G/BSA calculations
Hyperlipedemia

A B S T R A C T

Phytochemicals, have long been studied for various severe metabolic illnesses and degenerative diseases like heart disease and cancer because of their significant therapeutic effects. In animal cells, cholesterol serves a critical role being a component of cell membranes and essential for the normal functioning of precursor cells to some steroid hormones. Three-hydroxy-3-methyl glutaryl coenzyme A (HMG-CoA) is converted into mevalonate by the HMG-CoA Reductase (HMGCR) enzyme to produce cholesterol. However, when cholesterol levels are high, it may result in atherosclerosis. Statins, also known as synthetic drugs which decrease cholesterol, are therefore designed to work by targeting this enzyme. For patients with dyslipidemia, the side effects of excessive statin therapy have proven alarming hence using natural plant-based inhibitors is a promising alternative. Computational approach helps to identified many drugs that can target HMG-CO A Reductase. In this study, using *in-silico* molecular docking via auto-dock, 20 medicinal plants with 120 phytochemicals, reported as having antihyperlipidemic activity through deep literature study, were screened as HMG-CoA reductase enzyme inhibitors. The virtual molecular docking results reveals that five bioactive compounds; Sominone, Guggulsterone, Phytosterol, Withanolide A and Basilol, had higher binding affinities towards the HMG-CO A Reductase having binding energies of −9.33, −8.99, −8.87, −8.58, and −8.48 kcal/mol, respectively. ADMET properties of selected compounds were analysed using swiss adme tool. Results showed that out of five compounds three follow Lipinski rule of five, having ADMET properties. The HMG-CoA reductase-ligand complex's stability was validated by RMSD, RMSF, Rg, H-bond results and principal component analysis. The resulting trajectories of converged period of MD were further exploited in MM-P/G/BSA calculations to derive accurate estimates of binding free energies. This leads one to the conclusion that five phytochemicals, Sominone, Guggulsterone, Phytosterol, Withanolide A and Basilol can serve as potential inhibitors in regulating HMGCR's function may assist the development of effective anti-hyperlipedemic drugs.

1. Introduction

In mammals, cholesterol plays a vital role in homeostasis. Since it is a lipid, cholesterol cannot dissolve in the bloodstream, which is water-based, so it is transferred as lipoproteins that mix easily with the blood. When lipoproteins have a high ratio of protein to lipids (cholesterol and others), they are known as high-density lipoprotein (HDL) or good cholesterol and when this amount is small, it is called low-density lipoprotein (LDL) or bad cholesterol (Cerqueira et al., 2016). Hyperlipidemia is a metabolic disorder indicated by an increase in total cholesterol, low-density lipoprotein (LDL), triglycerides and a decrease in high-density lipoprotein (HDL) or a combination of both. Lipid peroxidation in hyperlipidemia plays a vital role in atherogenesis by increasing the lipid deposit in the arterial wall (Hasimun et al., 2018). According to

* Corresponding author.
E-mail address: kumarniki2003@gmail.com (A. Panwar).

https://doi.org/10.1016/j.amolm.2025.100086
Received 7 December 2024; Received in revised form 13 March 2025; Accepted 23 April 2025
Available online 9 May 2025

the World Health Organization (WHO), hyperlipidemia is a significant risk factor for cardiovascular disease. Stroke and coronary heart disease account for around 31 % of deaths from cardiovascular disease.

HMG-CoA Reductase (HMGCR), a key enzyme (anchored in the endoplasmic reticulum membrane) in cholesterol biosynthesis, catalyzes the reductive cleavage of HMG-CoA to mevalonate the precursor of cholesterol (Jasmine and Vanaja, 2013). Its catalytic portions form a protein tetramer containing four active sites at the interface of two monomers (Antonio et al., 2022). The inhibition of HMG-CoA reductase efficiently lowers cholesterol levels in humans and other animals by reducing endogenous cholesterol synthesis. This inhibition triggers a compensatory response involving the activation of sterol regulatory element-binding protein-2 (SREBP-2), which upregulates both the HMG-CoA reductase and LDL receptor. The upregulation of HMG-CoA reductase is a feedback mechanism attempting to restore cholesterol synthesis but does not directly contribute to the cholesterol-lowering effect. Conversely, the upregulation of LDL receptors enhances LDL clearance from the bloodstream, contributing to the reduction of circulating cholesterol levels (Baskaran et al., 2015). Statins are the most popular group of medications used to lower plasma LDL cholesterol and currently used for hypercholesterolemia which serves as effective competitive inhibitors of HMG-CoA reductase due to their structural similarity with HMG- CoA (Toppo et al., 2021). Like statins, the HMG moiety occupies the HMG-CoA binding pocket, and the nonpolar region partially occupies part of the coenzyme A binding site (Antonio and Villarreal-La Torre Víctor, 2022).

As first-line hyperlipidemic medications, statins also reduce vascular inflammation, the precursor to atherosclerosis (Blum, 2014). Therefore, there is great potential for developing alternative drugs inhibiting HMG-CoA reductase, especially from herbal medicines. Additionally, statins cause severe adverse effects, such as distal muscle weakness, headache, and acute renal failure. Side effects, such as hepatic transaminase elevation, sensory disturbances, and depression, have also been observed on prolonged use (Lin et al., 2015). For this reason, there is a growing interest in identifying reliable and effective alternatives to statin use that do not have or have low side effects (Ram et al., 2020). Additionally, traditional plant-based medicines have played a significant role in healthcare from ancient times. Numerous bioactive substances (isoflavones, diosgenin, resveratrol, quercetin, catechin, sulforaphane, and tocotrienols) typically derived from terrestrial plants, have been shown to lower the risk of cardiovascular diseases and support cardioprotection (Vasanthi et al., 2012). Testing drug candidates' activity and mechanism of action through an in-silico study has developed into a crucial and integral part of the drug discovery process. By predicting the binding affinity of drug candidates to specific receptors and optimizing their pharmacokinetic profile, in-silico techniques are usually used in the early stages of the drug discovery process. One of the methods in the in-silico study is molecular docking as a part of the structure-based drug design (Miladiyah and Nuryadi, 2022). Automated molecular docking software aims to understand and predict molecular recognition structurally, finding likely binding modes, and energetically, predicting binding affinity Morris and Lim-Wilby (2008) and use a scoring function that correctly ranks candidate dockings. The computational approaches include lead optimization, binding energy determination, and dynamic simulation studies but also the prediction of physicochemical and pharmacokinetic parameters of the small molecules. Several tools can be employed for this purpose, among which SwissADME is popular due to its free and open access to all (Bakchi et al., 2022).

The fundamental concept of molecular dynamics (MD) simulations is to model the motion of atoms and molecules over time by calculating the forces acting on each atom at successive time steps. These forces are used to update the positions and velocities of atoms according to Newton's equations of motion, providing insights into the dynamic behavior of molecular systems (Karplus and McCammon, 2002; Jorgensen, 1981; Lemkul, 2018). Notably, these simulations can also anticipate how biomolecules will react to alterations like mutation, phosphorylation, protonation, or the addition or removal of a ligand at the atomic level. Simulations determine the effects of numerous molecular perturbations by contrasting simulations run under various conditions (Hollingsworth and Dror, 2018).

These techniques include network theory, Markov state models, stochastic approaches like the Langevin equation, and a variety of dimensionality reduction techniques (Sittel et al., 2014). A multivariate statistical method, Principal Component Analysis (PCA), is used to systematically lower the number of dimensions required to characterize protein dynamics through a decomposition process that sorts observed motions from the largest to smallest spatial scales (David and Jacobs, 2014). Principal component analysis has become an increasingly popular technique for accounting for the integral dynamics of the system on a low-dimensional free energy landscape in molecular dynamics simulations.

2. Materials and methods

The computer system (Hp) Super Micro workstation, with the following specification properties; silver 4216 CPU, Intel® xenon ® @ 2.10 GHz with 32 cores, with NVIDIA Ge Force RTx 2080Ti Dual graphic cards, 128 Gigabyte RAM was used throughout the present study. The software downloads and installed include Ubuntu 18.04 LTS, Gromacs 2020, Auto- Dock 5.4109 software, Avogadro software, Discovery Studio Visualizer 2021, and Chimera version 1.16. online tools include SwissADME Tool, admet SAR tool, PRO TOX II and Galaxy online server.

2.1. Retrieval of target protein structure

The 3-D x-ray crystal structure file of the target enzyme: HMG-CoA reductase, with PDB ID-1HW8 and a high resolution of 2.10 Å, was retrieved from the RCSB PDB.

2.2. Selection and retrieval of ligand molecules

A dataset of 120 phytochemicals from 20 plants like Fenugreek (*Trigonella foenum*), Ashwagandha (*Withania somnifera)*, Cumin (*Cuminum cyminum*), Tulsi (*Ocimum basilicum*) etc., with potential antihyperlipidemic properties was made through a deep literature survey. Additionally, the structure of drug currently being used in the treatment of hyperlipidemia was also retrieved. The 2D and 3D structures of phytochemicals were obtained in SDF format from the PubChem database.

2.3. Moleculer docking

2.3.1. Target preparation

The Preprocessing of three-dimensional protein structures was performed using the Auto dock. The water molecules, ions, and bound ligands from the protein crystal structure were removed from the three-dimensional structure of HMGCR protein. Successively, the hydrogen atoms and Kollman charges were added to the three-dimensional structure of HMGCR protein. After preparation protein was saved in PDBQT format for performing molecular docking.

2.3.2. Ligand preparation

Ligand 3-D SDF structures were saved into Protein Data Bank (PDB) file format using open babel software 2.4.1 and whose 3-D SDF files were not available, their 2-D structures were retrieved and further converted to three-dimensional form using their SMILES through Open Babel.

The phytochemicals were prepared for docking by adding hydrogen, gasteiger charges and torsion through the Auto dock tool. The structures of phytochemicals were saved in pdbqt format for further study.

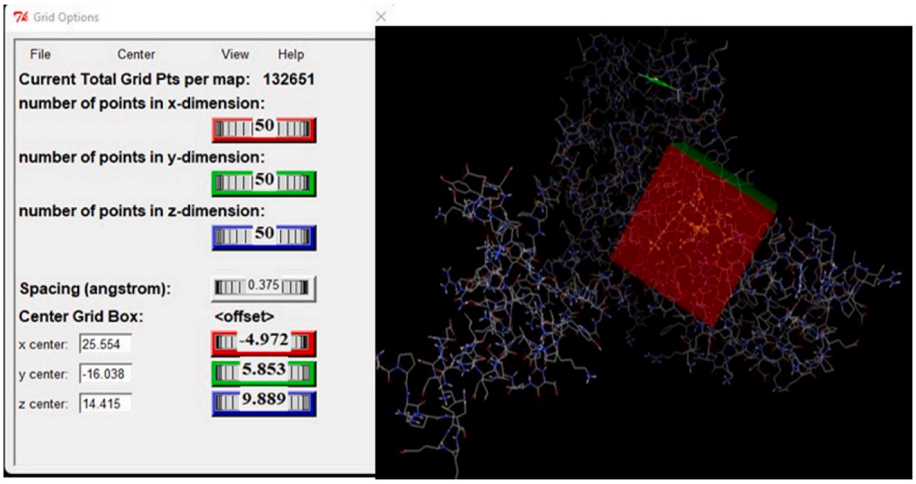

Fig. 1. Grid box parameters and Grid box over the target around a reference ligand.

2.3.3. Binding sites identification

The identification of active site was performed using UCSF Chimera. The amino acids from the active site were selected for the grid generation and docking.

2.3.4. Grid generation

Grid box was generated based on selecting amino acids of active/binding sites of target protein whose coordinates were: Center_x = 25.554, Center_y = −16.038, Center_z = 14.415 and the dimensions of the grid box were, X: 50, Y: 50 and Z: 50 (unit of the dimensions, Å) (see Fig. 1).

2.3.5. Molecular docking

Auto Dock (with default values for parameters) was used for molecular docking studies to explore all possible orientations and binding affinities for the ligand with the amino acids within the active site of target proteins.

2.3.6. Selection of the most active conformation

Upon successful molecular docking, the protein-ligand docked complexes were analysed based on docking score and binding affinities, a more negative value means a greater affinity. The conformations with lower binding energy as compared to the known drug of the target receptor chosen for further analysis.

2.3.7. Protein-ligand interactions

In the end, the top score results were visualized for the non-bonding interactions between the docked protein–ligand complex and to analyze the docking pose by Biovia Discovery Studio (2021). The 2-D diagram shows the various amino acid residues and the types of bonds that occur. Visualization of all ligands for hydrophobicity was performed by program UCSF Chimera 1.16.

2.4. Molecular dynamics simulation

Ligands showing the highest binding affinity were subjected to molecular dynamics simulations using the GROMACS 2020.3 package. This software incorporates key algorithms such as the Verlet leapfrog integrator for time integration (Swope et al., 1982) and the Particle-Mesh Ewald (PME) method for accurately computing long-range electrostatic interactions (Darden et al., 1993). The system was equilibrated under both NVT (constant Number, Volume, and Temperature) and NPT (constant Number, Pressure, and Temperature) ensembles, ensuring temperature and pressure stability, respectively. The NVT ensemble maintained the system at a temperature of 300 K using the velocity-rescaling thermostat (Bussi et al., 2007), while the NPT ensemble stabilized the pressure at 1.0 bar using the Parrinello-Rahman barostat (Parrinello and Rahman, 1981). These conditions provided a realistic simulation environment mimicking physiological conditions (Hollingsworth and Dror, 2018).

2.4.1. Generating topology

Protein topology was generated by using all-atom CHARMM36 force field with TIP3P water model while ligand topology files were generated through Swiss Param web server.

2.4.2. Simulation box and solvation

The protein was placed at the center of 351.628 dodecahedron box with 1.0 nm away from the box's edge. The system was solvated with the TP3P water model, and the charges of the system were neutralized upon adding Na+ and Cl− with 0.1 M ionic strength.

2.4.3. Energy minimization

Energy minimization was done by steepest descent method with the maximum gradient of 1000 kJ/mol/nm 50,000 iteration steps to reduce the steric clashes.

2.4.4. Equilibration

Temperature, pressure, and density were stabilized to 300 K, 1.0 bar and 1023 kg/m^3, respectively over time. Trajectory structures were stored at every 10ps.

2.5. Binding energy calculations using MM/PB/GBSA

The MMPBSA binding free energy of receptor-ligand docked complexes was estimated using the gmx_MMPBSA module, which utilized the MD simulation trajectories.

The binding energy was computationally calculated using the following:

$$\Delta Gbind = \Delta GRL - \Delta GR - \Delta GL$$

2.6. Principal component analysis

A covariance matrixA covariance matrix can describe the correlated internal motion of a molecule.

Diagonalization of this covariance matrix results in 3 N eigenvectors and eigenvalues, which describe the modes of the collective motion and their respective amplitudes. To analyze the collective motion of all

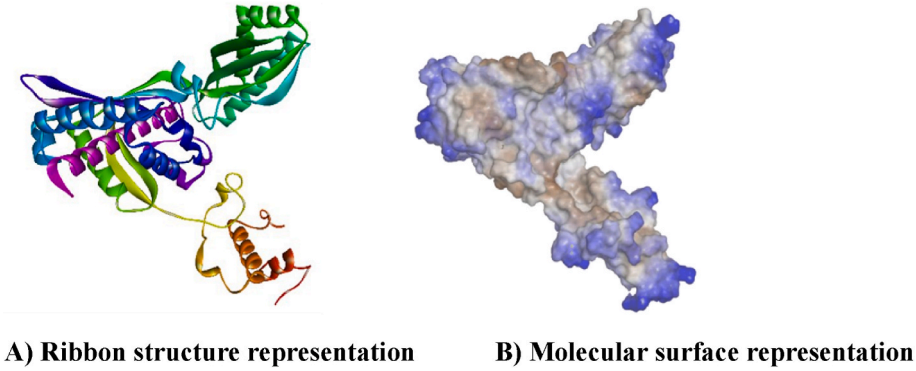

Fig. 2. Crystal structure of HMG-CO A Reductase with PDB ID:1HW8. A) Ribbon structure representation B) Molecular surface representation.

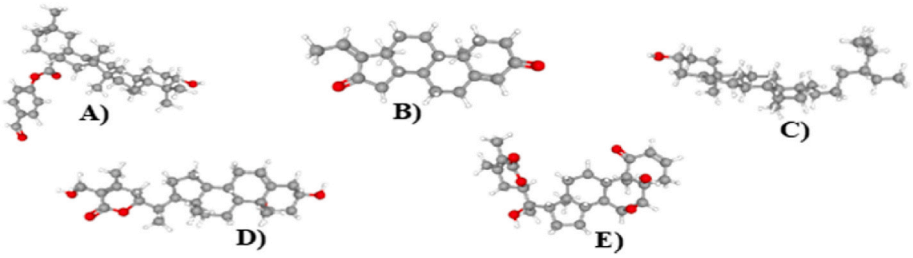

Fig. 3. 3D sdf structures of some phytochemicals retrieved from pubchem database A) Basilol B) Guggulsterone C) Phytosterol D) Sominone E) Withanolide-A.

complexes, we performed the PCA analysis based on C-α atoms by:

I. Computing the covariance matrix
II. Computing eigen vectors of the covariance matrix
III Transforming Data using eigen vectors
IV. Scatter plot of transformed data

All these steps were performed using galaxy Bio-3D server and graphs were generated with information about the proportion of variance in the complexes.

2.7. ADME-T properties prediction

The best-docked complexes were then evaluated for drug-like properties Absorption, Distribution, Metabolism, Excretion, and Toxicity of molecules were determined using ADME-T prediction tools such as such as SwissADME (http://www.swissadme.ch/index.php). Toxicity analysis was performed using the tool admetSAR (http://lmmd.ecust.edu.cn/admetsar2).

3. Results

The current investigation aimed to find potential chemical compounds that can bind to human HMG-CO A Reductase and serve as potent inhibitors through molecular docking and ADMET predictions. In this study, 120 phytochemicals were examined that have been previously identified as having antihyperlipidemic action.

3.1. Retrieval of the target structure

3.2. Selection and retrieval of ligand molecules

3.3. Dataset of phytochemicals

A dataset containing 120 phytochemicals with anti-hyperlipedemic activities was created (Table 1). The plant sources selected for phytochemicals included Ajowain, Fenugreek, Ginger, Saffron, Tamarind, Turmeric, among others. Additionally standard drug Atorvastatin was included in the dataset (see Fig. 3).

3.4. Binding site identification

The native and co-crystallized ligand with the protein HMGCR was compacting (Fig. 4). The amino acids located at the identified active site and docking of HMGCR were ARG590, GLU665, VAL683, SER684, ASN686, LYS688, ASP690, LYS691 and LYS692.

3.5. Molecular docking of HMG-CoA reductase and ligand compounds

A total of 120 phytochemcials were docked against HMGCR using Auto Dock 1.6 software platform. The most potent inhibitor, atorvastatin, was docked into the active site of HMG-CoA reductase (PDB ID-1HW8). Atorvastatin was assigned as a reference compound to compare its binding mode with hit compounds and to select final hits from the docking studies. Table 2 listed the docking score and binding energies of docked complexes. The results of molecular docking show a comparison of the docking scores of a compound with other compounds, and it can explain whether a compound has potential or not. Molecules with the lowest docking score (minus value) showed a high binding affinity.

3.6. Ranking of phytochemicals based on molecular docking results

All the docked phytochemicals were ranked in increasing order of their respective binding energies followed by ligand efficiency, inhibitory constant and no. of hydrogen bonds formed.

Table 1
List of phytochemicals with their plant sources selected based on hyperlipidemic activity.

Phytochemicals	Molecular formula	Molecular Weight(g/mol)	PubChem ID	Reference
1.Garlic (*Allium sativum*)				Tigu et al., 2021
Allicin	C6H10OS2	162.3	65036	
Isoquercitrin	C21H20O12	464.4	5280804	
p-Coumaric acid	C9H8O3	164.16	637542	
Gentisic acid	C7H6O4	154.12	3469	
Quercetin	C15H10O7	302.23	5280343	
2. Ashwagandha (*Withania somnifera)*				Saleem et al. (2020)
Oleic acid	C18H34O2	282.5	445639	
Withanone	C28H38O6	470.6	21679027	
Sominone	C28H42O5	458.6	44249449	
Withanolide A	C28H38O6	470.6	11294368	
Hygrine	C8H15NO	141.21	440933	
Withasomnine	C12H12N2	184.24	442877	
Anaferine	C13H24N2O	224.34	443143	
3.Bhringraj (*Eclipta alba*)				Mithun et al. (2011)
Sclerosol	C2H6OS	78.14	679	
Phytosterol	C29H50O	414.7	124823816	
Carbamic acid	CH3NO2	61.04	277	
Ursolic acid	C30H48O3	456.7	64945	
Acetamide	C2H5NO	59.07	178	
4. Amla (*Emblica officinalis*)				Hashem-Dabaghian et al., 2018
Pyrogallol	C6H6O3	126.11	1057	
Ellagic acid	C14H6O8	302.19	5281855	
Chebulic acid	C14H12O11	356.24	71308174	
Citric acid	C6H8O7	192.12	311	
Kaempferol	C15H10O6	286.24	5280863	
Mucic acid	C6H10O8	210.14	3037582	
5. Flaxseed *(Linum usitatissimum)*				Pansare et al. (2020)
Ferulic acid	C10H10O4	194.18	445858	
hexadecanoic acid	C16H32O2	256.42	985	
pinoresinol	C20H22O6	358.4	73399	
6. Turmeric (*Curcuma longa*)				Chanda and Ramachandra, 2019
Curcumin	C21H20O6	368.4	969516	
Eugenol	C10H12O2	164.2	3314	
Pcymene	C10H14	134.22	7463	
1,8-cineole	C10H18O	154.25	2758	
Beta-pinene	C10H16	136.23	14896	
Beta-Turmerone	C15H22O	218.33	196216	
Limonene	C10H16	136.23	22311	
Niacin	C6H5NO2	123.11	938	
7. Guggul (*Commiphora wightii*)				Sarup et al. (2015)
Guggulsterol-I	C27H44O4	432.6	101297673	
Guggulsterone	C21H28O2	312.4	3084731	
Mansumbinone	C22H34O	314.5	128179	
Commiferin	C15H20O3	248.32	91864439	
Myrrhanone A	C30H50O3	458.7	102242791	
8. Fenugreek (*Trigonella foenum*)				Shahidi and Hossain (2018)
Naringenin	C15H12O5	272.25	439246	
Vitexin	C21H20O10	432.4	5280441	
Estragol	C10H12O	148.2	8815	
Saponaretin	C21H20O10	432.4	162350	
Trans-anethole	C10H12O	148.2	637563	
9. Tulsi (*Ocimum basilicum*)				Marwat et al. (2011)
Alpha-phellandrene	C10H16	136.23	7460	
Terpinolene	C10H16	136.23	11463	
Cis-ocimene	C10H16	136.23	5320250	
linalool	C10H18O	154.25	6549	
Nerol	C10H18O	154.25	643820	
Verbenone	C10H14O	150.22	29025	
Basilol	C37H52O4	560.8	16655699	
Cadinene	C15H26	206.37	3032853	
Alpha-gurjunene	C15H24	204.35	15560276	
Piperitone	C10H16O	152.23	6987	
Thymol	C10H14O	150.22	6989	
10. Coriander (*Coriandrum sativum*)				Sobhani et al. (2022)
Citronellal	C10H18O	154.25	7794	
Camphor	C10H16O	152.23	2537	
Geraniol	C10H18O	154.25	637566	
Anethole	C10H12O	148.2	637563	
Decanal	C10H20O	156.26	8175	
Apigenin	C15H10O5	270.24	5280443	
Luteolin	C15H10O6	286.24	5280445	
Coumarin	C9H6O2	146.14	323	
11. Arjuna (*Terminalia arjuna*)				Gupta et al. (2018)

(*continued on next page*)

Table 1 (*continued*)

Phytochemicals	Molecular formula	Molecular Weight(g/mol)	PubChem ID	Reference
Terminic acid	C30H48O4	472.7	132568257	
Arjunone	C19H20O6	344.4	14034821	
Baicalein	C15H10O5	270.24	5281605	
Pelargonidin	+C15H11O5	271.24	440832	
Ethyl gallate	C9H10O5	198.17	13250	
Oleanolic acid	C30H48O3	456.7	10494	
12. Ajwain (*Thymus vulgaris*)				Hossain and Shahidi (2023)
Hexadecanal	C16H32O	240.42	984	
Cyclohexane	C6H12	84.16	8078	
Phytol	C20H40O	296.5	5280435	
Aromadendrene	C15H24	204.35	91354	
Caryophyllene	C15H24	204.35	5281515	
Humulene	C15H24	204.35	5281520	
13. Clove (*Syzygium aromaticum*)				El-SaberBatiha et al., 2020
Crategolic acid	C30H48O4	472.7	73659	
Biflorin	C16H18O9	354.31	441959	
Rhamnetin	C16H12O7	316.26	5281691	
Eugenitin	C12H12O4	220.22	3083581	
Carvacrol	C10H14O	150.22	10364	
Caempesterol	C28H48O	400.7	173183	
Eugenin	C11H10O4	206.19	10189	
14. Rosemary (*Rosemarinus officinalis*)				Amar et al. (2017)
Rosmarinic acid	C18H16O8	360.3	5281792	
Rosmanol	C20H26O5	346.4	13966122	
Carnosol	C20H26O4	330.4	442009	
Cirsimaritin	C17H14O6	314.29	188323	
Genkwanin	C16H12O5	284.26	5281617	
Scutellarein	C15H10O6	286.24	5281697	
15. White poppy (*Papaver somniferum*)				Butnariu et al. (2022)
Coclaurine	C17H19NO3	285.34	160487	
Reticuline	C19H23NO4	329.4	439653	
Scoulerine	C19H21NO4	327.4	22955	
Papaverine	C20H21NO4	339.4	4680	
Glaucamine	C21H23NO6	385.4	609842	
16. Saffron (*Crocus sativus*)				Pansare et al. (2020)
Gallic acid	C7H6O5	170.12	370	
Caffeic acid	C9H8O4	180.16	689043	
Safranal	C10H14O	150.22	61041	
Picrocrocin	C16H26O7	330.37	130796	
Cinnamic acid	C9H8O2	148.16	444539	
17. Tamarind (*Tamarindus indica*)				Pansare et al. (2020)
Epicatechin	C15H14O6	290.27	72276	
Taxifolin	C15H12O7	304.25	439533	
Catechin	C15H14O6	290.27	9064	
Furfural	C5H4O2	96.08	7362	
2-phenyl-acetaldehyde	C8H8O	120.15	998	
18. Cumin (Cuminum cyminum)				Chouhan et al., 2022
Ethyl oleate	C20H38O2	310.5	5363269	
Cuminaldehyde	C10H12O	148.2	326	
Methyl linoleate	C19H34O2	294.5	5284421	
Dihydrojasmone	C11H18O	166.26	62378	
Biformene	C20H32	272.5	23252995	
Cumic acid	C10H12O2	164.2	10820	
19. Saunf (*Foeniculum vulgare*)				Foroughi et al. (2016)
Camphene	C10H16	136.23	6616	
Germacrene D	C15H24	204.35	5317570	
Fenchone	C10H16O	152.23	14525	
Cis-anethole	C10H12O	148.2	1549040	
20. Ginger (*Zingiber officinale*)				Ashraf et al. (2017)
6-gingerol	C17H26O4	294.4	442793	
6-shogaol	C17H24O3	276.4	5281794	
8-paradol	C19H30O3	306.4	213821	
10-gingeridone	C21H32O4	348.5	5317591	
Citronellyl acetate	C12H22O2	198.3	9017	
β-sesquiphellandrene	C15H24	204.35	12315492	
Copaene	C15H24	204.35	12303902	
Atorvastatin	C33H35FN2O5	**558.6**	**60823**	

3.7. Molecular docking results were analysed based on following factors

3.7.1. Binding energy

From the docking results, binding free energies were observed from lowest to highest values. Results showed that the total score ranged from −2.83 for acid to −9.33 for sominone (Table 2). Out of 120 phytochemical compounds, top 14 hits were found, Sominone (−9.33), Guggulsterone (−8.99), Phytosterol (−8.87), Withanolide A (−8.58), Basilol (−8.48), Caempsterol (−8.07), Curcumin (−7.72), Glaucamine (−7.69), Isoquercitrin (−7.66), Coclaurine (−7.66), Vitexin (−7.6), Crategolic acid (−7.57), Copaene (-7.43) and Papaverine (−7.36) exhibited stronger binding affinity than reference ligand compound

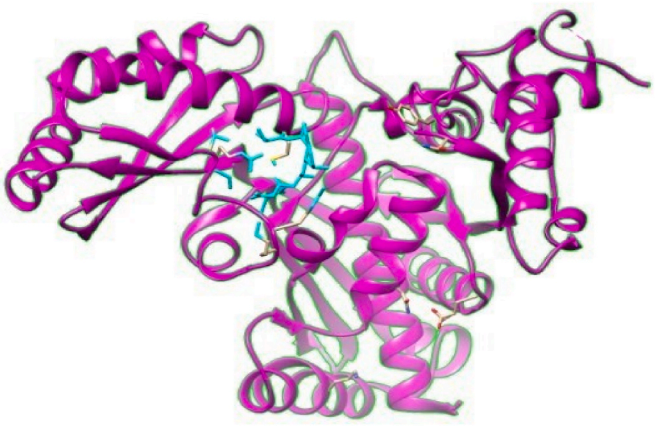

Fig. 4. Three-Dimensional crystal structure of selected target protein with co-crystallized inhibitor/ligand.

atorvastatin (−7.31).

3.7.2. Hydrogen bond interactions

Are essential in determining the binding affinity and stability of complexes. Isoquercitrin & Rosmarinic acid formed a maximum no of H-bonds (7), Vitexin, Ellagic acid, and Gallic acid formed 5 H-bonds, Scutellarein, Rosmanol, Baicalein, Caffeic acid, Gentisic acid, Ethyl gallate, Chebulic acid and Citric acid formed 4 H-bonds and the statin formed 4 H-bonds. Statin interacted through LYS691, LYS692, GLN770, ASP767 amino acid residues and there are several compounds those give similarity of binding amino acid residues with statin drug (Atorvastatin) as the original ligand of HMG-CoA Reductase. Ursolic acid and pinoresinol interacted through LYS691, while picrocrocin interacted through LYS692.

3.7.3. Ligand efficiency (LE) and inhibition constant (Ki)

The Ki shows that the inhibitors' efficacy is good. For the five compounds, the values range from −0.21 to −0.39 kcal/mol/non-hydrogen atoms. However, LE is the ligand's capacity to induce a biological reaction when bound to the target receptor (Table 2). The LE range from good to excellent is less than 0.4 and varies during the drug discovery process.

The study reveals that most of our screened phytochemical compounds exhibited strong binding with target protein at the inhibitory binding site compared to positive control drugs.

3.8. Protein-ligand interactions

Out of 120 ligands screened against HMG-CO A Reductase, the top five potential candidates, Sominone, Guggulsterone, Phytosterol, Withanolide A and Basilol, were selected for further analysis and visualization by Discovery Studio (https://discover.3ds.com/discovery-studio-visualizer-download) (Figs. 5–10) which had binding affinities of −9.33, −8.99, −8.87, −8.58, and −8.48 kcal/mol, respectively (Table 3) (see Fig. 2).

The amino acid residues involved in the hydrogen bond and hydrophobic interactions in docked complexes (Table 4).

3.9. Visualization of protein-ligand interactions using biovia Discovery Studio 2021

The major interactions found during visualization include pi-sigma (help ligands intercalate at receptor binding sites), hydrogen (provides stability to the complex), and pi-alkyl (contributes the ligand's dipole moment for the molecule's orientation) bonds. Each bond in the target protein serves followings are the function.

Table 2
Binding energy of phytochemicals docked against HMG-CoA Reductase.

S. No	Ligand	Binding Energy (kcal/mol)	Ligand efficiency	Inhibitory Constant (uM)	No of H bonds
1	Sominone	−9.33	−0.28	0.14	2
2	Guggulsterone	−8.99	−0.39	0.25	1
3	Phytosterol	−8.87	−0.3	0.31	1
4	Withanolide A	−8.58	−0.25	0.51	4
5	Basilol	−8.48	−0.21	0.61	3
6	Caempsterol	−8.07	−0.28	1.21	1
7	Curcumin	−7.72	−0.29	2.18	3
8	Glaucamine	−7.69	−0.27	2.32	2
9	Isoquercitrin	−7.66	−0.23	2.44	7
10	Coclaurine	−7.66	−0.36	2.44	3
11	Vitexin	−7.6	−0.25	2.7	5
12	Crategolic acid	−7.57	−0.22	2.82	1
13	Copaene	−7.43	−0.5	3.59	0
14	Papaverine	−7.36	−0.29	4	1
15	Luteolin	−7.31	−0.35	4.39	3
16	Rhamnetin	−7.31	0.32	4.35	3
17	**Atorvastatin**	**−7.31**	**−0.18**	**4.4**	**4**
18	Biformene	−7.28	−0.36	4.64	0
19	Kaempferol	−7.25	−0.35	4.82	3
20	Cirsimaritin	−7.25	−0.32	4.85	3
21	Scutellarein	−7.23	−0.34	5.06	4
22	Rosmarinic acid	−7.22	−0.28	5.1	7
23	Rosmanol	−7.22	−0.29	5.12	4
24	Beta-Turmerone	−7.21	−0.45	5.23	1
25	Cadinene	−7.19	−0.48	5.42	0
26	Naringenin	−7.15	−0.36	5.71	2
27	Germacrene D	−7.13	−0.48	5.96	0
28	Epicatechin	−7.12	−0.34	6.06	3
29	Baicalein	−7.11	−0.36	6.13	4
30	Commiferin	−7.1	−0.39	6.24	3
31	Oleanolic acid	−7.08	−0.21	6.49	1
32	Myrrhanone A	−7.06	−0.21	6.64	2
33	Mansumbinone	−7.05	−0.31	6.78	0
34	Genkwanin	−7.02	−0.33	7.19	3
35	Ellagic acid	−7.01	−0.32	7.26	5
36	Taxifolin	−6.99	−0.32	7.47	2
37	Beta -sesquiphellandrene	−6.98	−0.47	7.65	0
38	6-shogaol	−6.91	−0.35	8.66	3
39	Apigenin	−6.9	−0.35	8.57	2
40	Catechin	−6.88	−0.33	9.08	2
41	Scoulerine	−6.8	−0.28	10.34	2
42	Guggulsterol-I	−6.79	−0.22	10.55	2
43	Aromadendrene	−6.72	−0.45	11.96	0
44	Arjunone	−6.71	−0.27	12.07	2
45	Terminic acid	−6.61	−0.19	14.22	0
46	Caryophyllene	−6.6	−0.44	14.55	0
47	Saponaretin	−6.59	−0.21	14.69	3
48	Eugenitin	−6.57	−0.41	15.39	2
49	Withanone	−6.55	−0.47	15.89	1
50	Withasomnine	−6.55	−0.47	15.88	1
51	Reticuline	−6.55	−0.27	15.86	2
52	Caffeic acid	−6.46	−0.5	18.33	4
53	Humulene	−6.33	−0.42	23.24	0
54	Biflorin	−6.33	−0.25	22.93	3
55	Ferulic acid	−6.28	−0.45	24.94	3
56	Eugenin	−6.26	−0.42	25.98	1
57	Piperitone	−6.2	−0.56	28.35	1
58	6-gingerol	−6.13	−0.29	31.87	2
59	Gentisic acid	−6.09	−0.55	34.46	4
60	Ursolic acid	−6.07	−0.18	35.75	3
61	Alpha-gurjunene	−6.05	−0.4	36.94	0
62	10-gingeridone	−6.04	−0.24	37.09	1
63	Verbenone	−6.01	−0.55	39.1	1
64	Coumarin	−5.98	−0.54	41.72	3
65	Quercetin	−5.87	−0.27	49.66	3
66	8-paradol	−5.77	−0.26	58.63	1
67	P-Coumaric acid	−5.74	−0.48	62.22	2
68	Safranal	−5.72	−0.5	64.34	1
69	Cumic acid	−5.69	−0.47	67.69	2
70	Eugenol	−5.67	−0.47	70.25	1

(continued on next page)

Table 2 (*continued*)

S. No	Ligand	Binding Energy (kcal/mol)	Ligand efficiency	Inhibitory Constant (uM)	No of H bonds
71	Camphor	−5.66	−0.51	70.54	1
72	Cinnamic acid	−5.66	−0.51	71.04	22
73	Dihydrojasmone	−5.65	−0.47	72.14	1
74	1,8-cineole	−5.63	−0.51	75.19	0
75	Beta-pinene	−5.63	−0.56	74.8	0
76	Citronellyl acetate	−5.61	−0.4	77.22	2
77	Geraniol	−5.6	−0.51	78.96	2
78	Ethyl gallate	−5.58	−0.4	81.87	4
79	Nerol	−5.53	−0.5	88.38	2
80	Thymol	−5.52	−0.5	90.4	2
81	Camphene	−5.47	−0.55	97.95	0
82	Anethole	−5.46	−0.5	99.6	1
83	Carvacrol	−5.44	−0.49	103.3	2
84	*Trans*-anethole	−5.41	−0.45	108.92	2
85	Cuminaldehyde	−5.36	−0.49	118.53	1
86	Fenchone	−5.35	−0.49	119.55	1
87	Terpinolene	−5.33	−0.53	124.67	0
88	Citronellal	−5.28	−0.48	135.47	1
89	*Cis*-anethole	−5.24	−0.48	143.14	1
90	Alpha-phellandrene	−5.22	−0.52	149.37	0
91	linalool	−5.19	−0.47	157.31	1
92	Estragol	−5.17	−0.47	161.59	1
93	Oleic acid	−5.14	−0.26	170.66	2
94	*Cis*-ocimene	−5.14	−0.51	169.58	0
95	Gallic acid	−5.12	−0.43	177.22	5
96	Anaferine	−5.04	−0.32	201.43	2
97	hexadecanoic acid	−5.03	−0.28	206.22	2
98	2-phenyl-acetaldehyde	−5.03	−0.56	204.22	1
99	Methyl linoleate	−5	−0.24	216.4	1
100	Limonene	−4.97	−0.5	228.79	0
101	Hexadecanal	−4.91	−0.29	253.43	1
102	Ethyl oleate	−4.84	−0.22	285.57	2
103	Hygrine	−4.56	−0.46	451.14	3
104	Pyrogallol	−4.55	−0.51	464.32	2
105	Pinoresinol	−4.55	−0.18	465.97	1
106	Allicin	−4.33	−0.48	666.12	1
107	Niacin	−4.26	−0.47	750.67	2
108	Pelargonidin	−4.17	−0.21	872.24	3
109	Chebulic acid	−4.09	−0.16	1000	4
110	Carbamic acid	−4.06	−1.01	1070	3
111	Furfural	−4.06	−0.58	1060	1
112	Decanal	−4.02	−0.37	1130	1
113	Cyclohexane	−3.98	−0.66	1210	0
114	Carnosol	−3.95	−0.16	1280	2
115	Picrocrocin	−3.94	−0.17	1290	0
116	Citric acid	−3.8	−0.29	1650	4
117	Acetamide	−3.72	−0.93	1870	2
118	P-cymene	−3.63	−0.36	2200	0
119	Sclerosol	−3.54	−0.89	2550	2
120	Phytol	−3.42	−0.16	3130	1
121	Mucic acid	−2.83	−0.2	8420	3

3.10. Molecular dynamics simulation

The top five best docked ligand–protein complexes Sominone, Guggulsterone, Phytosterol, Withanolide A and Basilol, were further analysed for the molecular dynamic simulations. The RMSD, RMSF, RG and SASA calculations were used to analyze the conformational stability and fluctuations under the simulated conditions. The best docked conformation of each compound including reference compounds were used as the initial structure for 50 ns MD simulations to refine their binding conformation.

3.11. The root mean square deviation (RMSD)

The stability of the docked protein-ligand complex is represented by its RMSD. The RMSD plot of the protein and docked complexes was calculated for 50 ns trajectory. RMSD analysis is done to examine various fluctuations within the complex during the simulation period. We observed that the largest deviation for Atorvostatin (black) was between 15 ns and 45 ns, resulting in an average change in RMSD of 0.5–0.75 nm (Fig. 11). The RMSD analysis of atorvastatin, despite being a standard drug, exhibited notable fluctuations, particularly after 20 ns of simulation. This is an unexpected outcome, as a well-established drug like atorvastatin is typically assumed to maintain a steady binding conformation. However, these fluctuations do not necessarily indicate that the simulation duration is insufficient. Instead, they may stem from the initial ligand conformation, the flexible nature of atorvastatin, or its dynamic interactions within the binding pocket. Previous studies have reported similar RMSD variations for atorvastatin, even in extended simulations beyond 100 ns (Kumari et al., 2021; Singh and Sharma, 2020), indicating that the observed instability is an inherent characteristic rather than a limitation of the simulation time. Phytosterol, shows a considerable variation around the initial 5 ns and 40 ns. The lack of stabilization of phytosterol after 40 ns is not due to its intrinsic molecular flexibility, transient binding interactions, and active site adaptability. Phytosterols can remain mobile within the binding pocket, leading to observed RMSD variations. This behavior suggests that phytosterols may bind in multiple conformations rather than a single, locked-in state. All the trajectories became stable after 40 ns until the end of the simulation study. The value of ligands RMSD of Sominone, Withanolide-A and Basilol was low as compared to Standard drug (Atorvastatin) RMSD indicates that ligands are more stable with the protein and its binding pocket.

The Root Mean Square Deviation (RMSD) graph depicts the structural deviations of the protein and its ligand-bound complexes over a 50 ns molecular dynamics simulation. The apoprotein, serving as a control, maintains a relatively stable RMSD, indicating its structural integrity in the absence of ligand binding. Among the ligand-bound systems, Atorvastatin exhibits lower RMSD fluctuations, suggesting a more stable interaction with the protein. In contrast, Guggulsterone and Phytosterol show higher fluctuations, implying significant conformational changes, possibly affecting binding stability. Withanolide-A exhibits moderate RMSD variations, implying that while it maintains relative stability, it undergoes some conformational shifts during the simulation. On the other hand, Basilol and Sominone maintain lower RMSD values, indicating that their binding induces fewer structural deviations compared to the unbound protein.

3.12. Root mean square fluctuation (RMSF)

Another key parameter that links the various amino acid residues, various peptide backbone regions, and trajectories is the RMSF. For the docked ligand complexes as well as the apoprotein, fluctuations in terms of amino acid residues were noted.

The RMSF values for the apoprotein (green) and the ligand-bound complexes were analysed to assess the impact of ligand binding on protein flexibility. The results indicate that while most complexes exhibited similar RMSF patterns along the amino acid residues, significant differences were observed for specific ligands. Guggulsterone (blue) displayed the highest RMSF values, particularly in the region spanning residues 750–800, suggesting that its binding induces substantial fluctuations in this segment. This could be indicative of weaker interactions or an allosteric effect leading to increased local flexibility. Withanolide-A (purple) also demonstrated moderate fluctuations in certain regions, though the degree of flexibility was lower than that of Guggulsterone. Based on the analysis of RMSF values, we can infer that all the predicted ligands exhibited minimal conformational changes during the binding process, indicating their potential to form stable complexes (Fig. 12).

3.13. Radius of gyration (RG)

Determines whether the complex remains stably folded or unfolds under simulated conditions over a 50 ns trajectory. Lower RG values

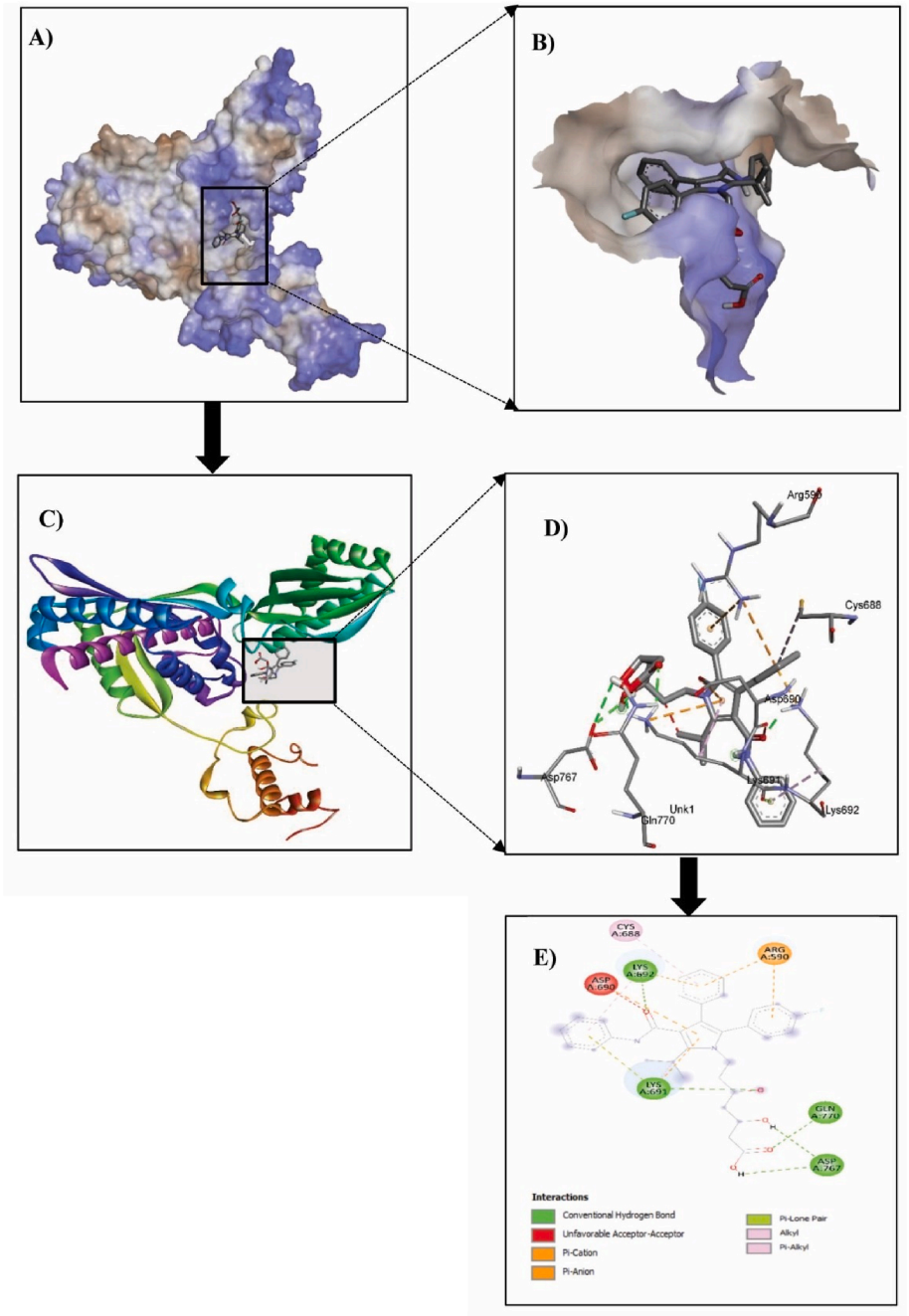

Fig. 5. Docking interaction of atorvastatin with HMG-coA Reductase (1HW8). (A) Moleculer surface of the docked complex. (B) The 3D hydrophobicity surface plot at the binding site. (C) Overall ribbon structure. (D) Ligand interactions with target protein. (E) 2-D interactions of the complex.

indicate tight packaging, suggesting a compact structure, while higher RG values suggest looser packing of the molecular structure. In molecular dynamics (MD) studies, RG is utilized to illustrate the influence of a ligand molecule on inducing conformational changes in the protein molecules (Fig. 13).

During the simulations, all complexes maintained a stable radius of gyration (RG) within the range of 2.5 nm–2.7 nm, indicating their stability throughout the simulation studies. Guggulsterone exhibited fluctuating radius of gyration (Rg) due to its impact on protein flexibility and transient binding interactions, causing periodic expansions and contractions. Its hydrophobic nature and steric effects likely disrupted structural packing, leading to instability. Additionally, possible allosteric effects or loop movements may have contributed to the dynamic shifts in protein compactness. The apoprotein maintained a relatively stable Rg, indicating that its native conformation remained compact throughout the simulation. Unlike Guggulsterone, it did not undergo significant structural fluctuations, suggesting an inherently stable folding pattern in the absence of ligand interactions. The stability of the apoprotein serves as a baseline reference, confirming that ligand-induced changes, such as those seen with Guggulsterone, were responsible for the observed fluctuations. The overall results suggest an increased compactness of both the protein and the docked structures, leading to enhanced stability during the simulation study.

3.14. Solvent accessible surface area

The solvent accessible surface area (SASA) is another significant parameter that quantifies the total area on the protein surface that is

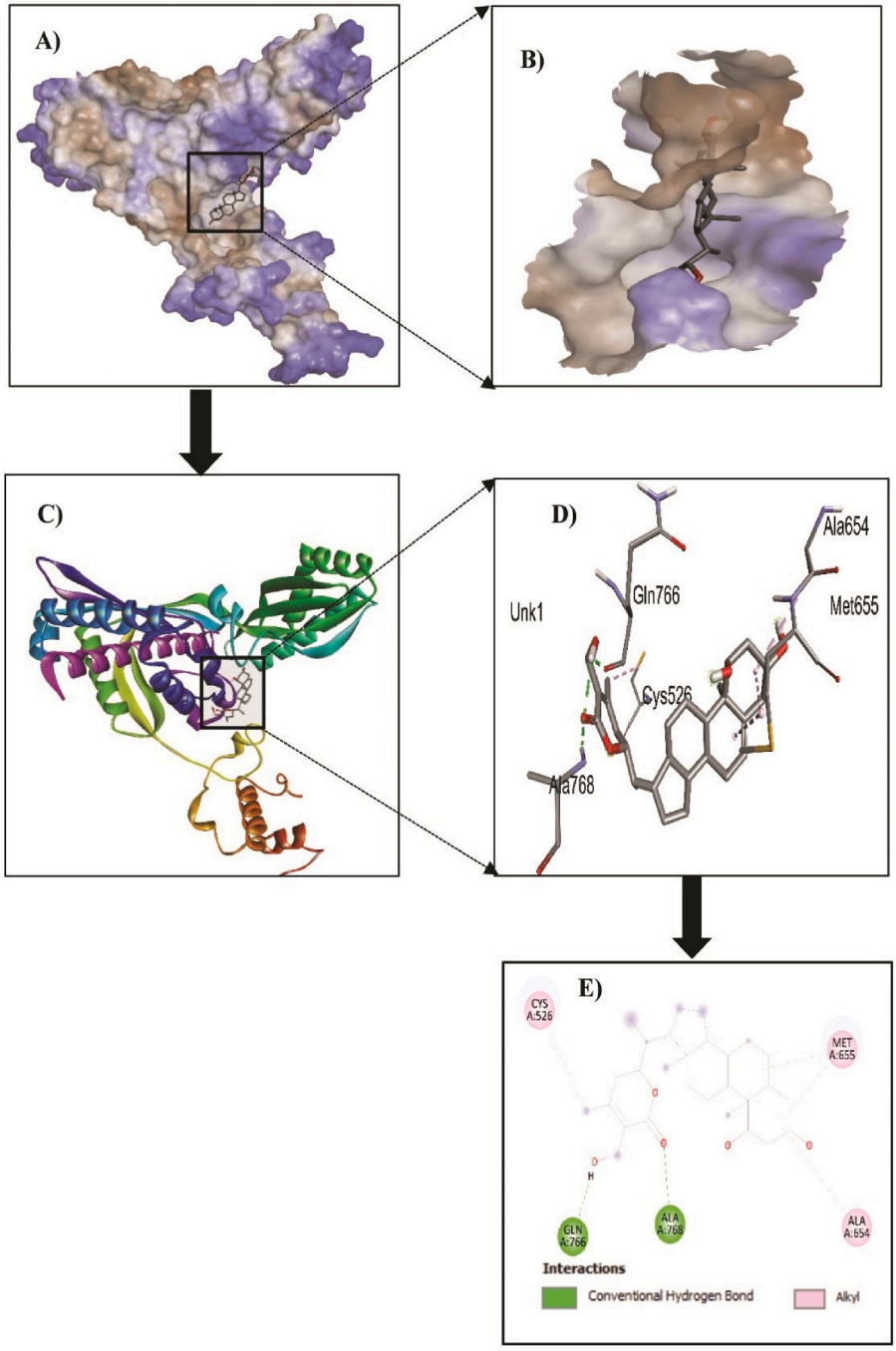

Fig. 6. Docking interaction of Sominone with HMG-coA Reductase (1HW8). (A) Moleculer surface of the docked complex. (B) The 3D hydrophobicity surface plot at the binding site. (C) Overall ribbon structure. (D) Ligand interactions with target protein. (E) 2-D interactions of the complex.

readily accessible to water solvents. A lower SASA value indicates minimal exposure of water solvent areas, thereby contributing to increased stability of the complex.

The trajectory plot showed that SASA value of all the complexes ranged between 195 nm^2 to 225 nm^2 highest being phytosterol, suggesting increased structural flexibility and solvent exposure and lowest for guggulsterone indicating a more compact structure with reduced solvent accessibility during the simulation (Fig. 14). The apoprotein remains relatively stable, indicating minimal conformational changes. These variations reflect the influence of ligand binding on protein stability and conformational dynamics.

3.15. Binding energy calcultions using MM/PB/GBSA

Accurate binding free energy estimation was calculated from Molecular Mechanics General Born/Poisson Boltzmann Surface Area (MM-GB/PBSA). This method of binding energy prediction was selected as it balances accuracy and computational power. The gmx_MMPBSA was used to separately minimize the receptor, ligand, and receptor-ligand complex using the below equation for the total binding free energy:

where,

$\Delta G(bind)$ = Binding free energy

G = Free energy of complex, protein, and ligand T = Temperature

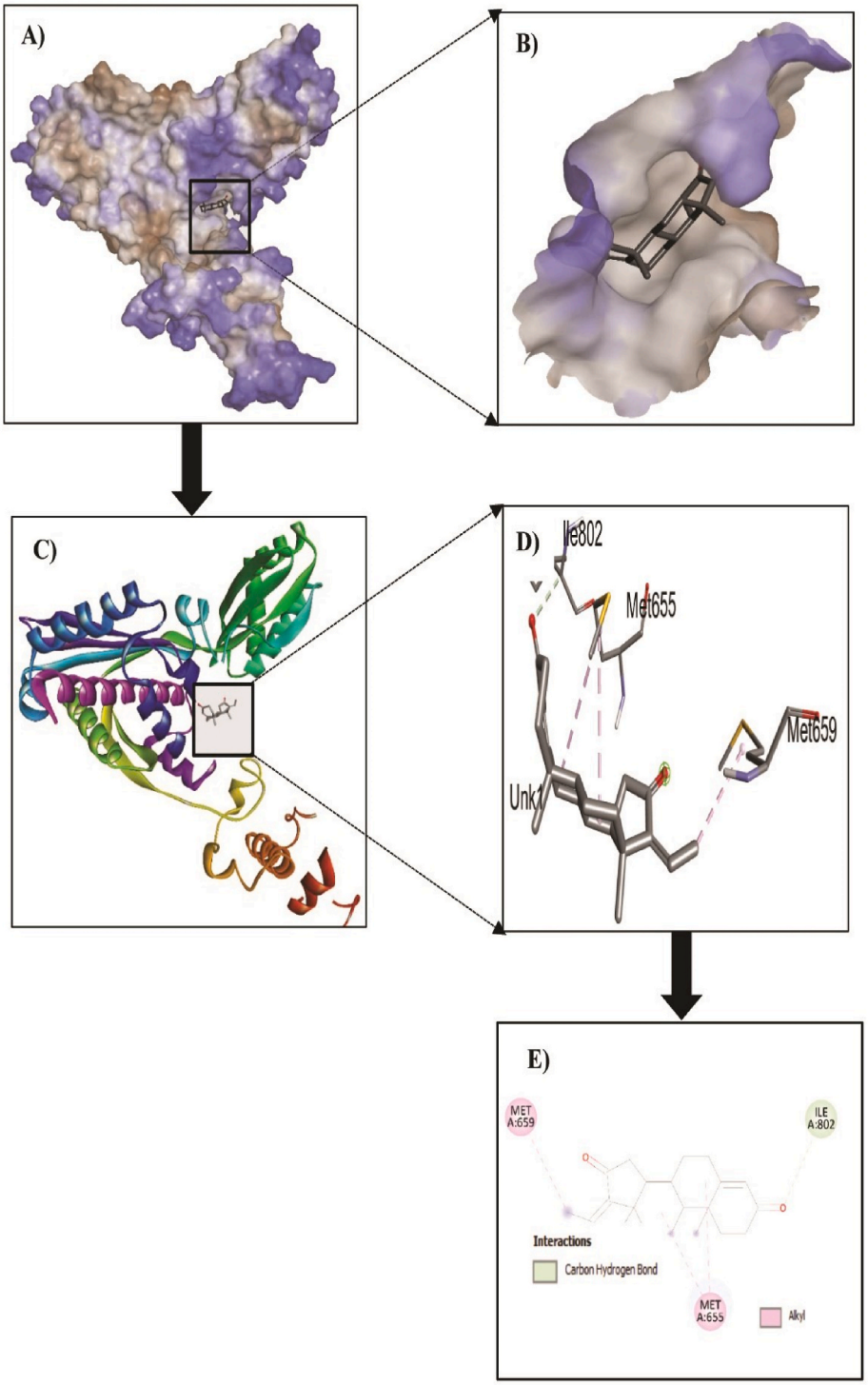

Fig. 7. Docking interaction of Guggulsterone with HMG-coA Reductase (1HW8). (A) Moleculer surface of the docked complex. (B) The 3D hydrophobicity surface plot at the binding site. (C) Overall ribbon structure. (D) Ligand interactions with target protein. (E) 2-D interactions of the complex.

ΔS = Entropy

ΔGgas = Gas phase molecule free energy

ΔGsolv = Solvation-free energy

ΔGGB = Polar solvation-free energy

ΔGSA = Non-polar solvation free energy

ΔG(bind) = Gcomplex – (Gligand + Greceptor)

ΔG = ΔGgas + ΔGsol – TΔS

ΔGgas = ΔEelectrostatic + ΔEvdW

ΔGsolv = ΔGGB + ΔGSA

Alongside the binding free energy, various other interaction energies, including van der Waals energy, electrostatic energy, polar solvation energy, and SASA energy, have been calculated for all complexes (Table 5). The results indicate that van der Waals, electrostatic, and SASA energies have a negative contribution to the total interaction

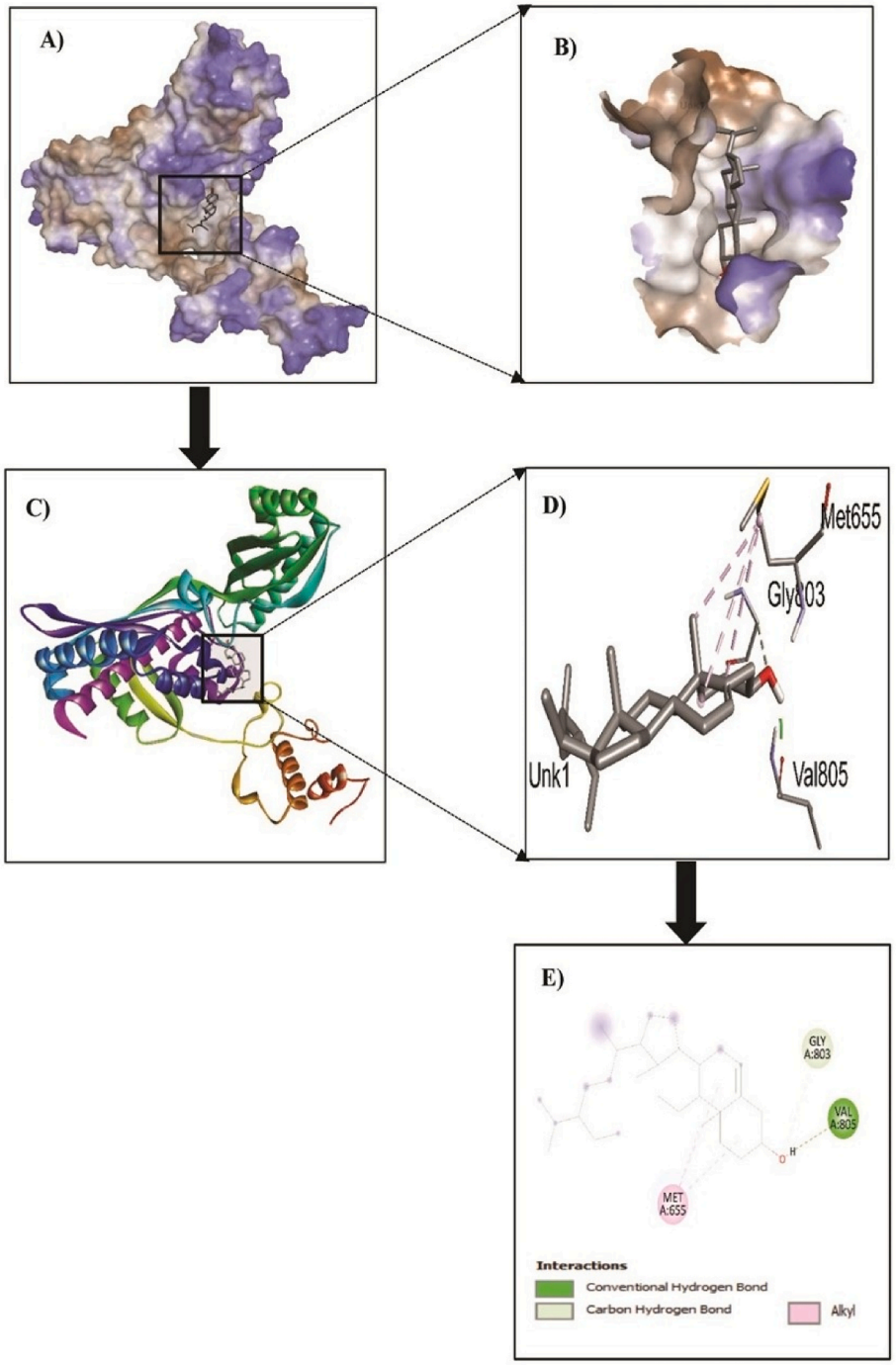

Fig. 8. Docking interaction of Phytosterol with HMG-CoA Reductase (1HW8). (A) Moleculer surface of the docked complex. (B) The 3D hydrophobicity surface plot at the binding site. (C) Overall ribbon structure. (D) Ligand interactions with target protein. (E) 2-D interactions of the complex.

energy, while only polar solvation energy has a positive contribution to the total binding free energy. The contribution of SASA energy to the total binding energy is relatively smaller. In complexes involving HMGCR, all ligands demonstrate that hydrophobic interactions play a crucial role in stabilizing the protein-ligand complex, as evident from the highly negative van der Waals energy values.

The MMGBSA analysis of HMG-CoA Reductase–ligand complexes (Fig. 15) indicates that Basilol exhibited the lowest binding free energy (−34.59 kcal/mol) among the test compounds, suggesting the highest binding affinity for the enzyme. This was followed by Withanolide-A (−30.24 kcal/mol), Phytosterol (−25.71 kcal/mol), Sominone (−22.62 kcal/mol), and Guggulsterone (−20.86 kcal/mol). In comparison, the standard drug Atorvastatin demonstrated the most favorable binding free energy overall (−39.42 kcal/mol), outperforming all test compounds in terms of binding affinity, except for Basilol, which showed a relatively comparable binding profile (refer to Table 5).

To enhance the binding affinity and binding energy, it is possible to optimize the structures of the compounds and refine the specific interactions between the ligands and the protein targets.

Several molecular mechanics force fields apply the Lennard-Jones function for describing the interaction energy between non-bonded neutral atoms.

LJ-SR: Protein-LIG reflects the VDW interaction, while Coul-SR reflects electrostatic interaction. The molecular dynamics performed at 50

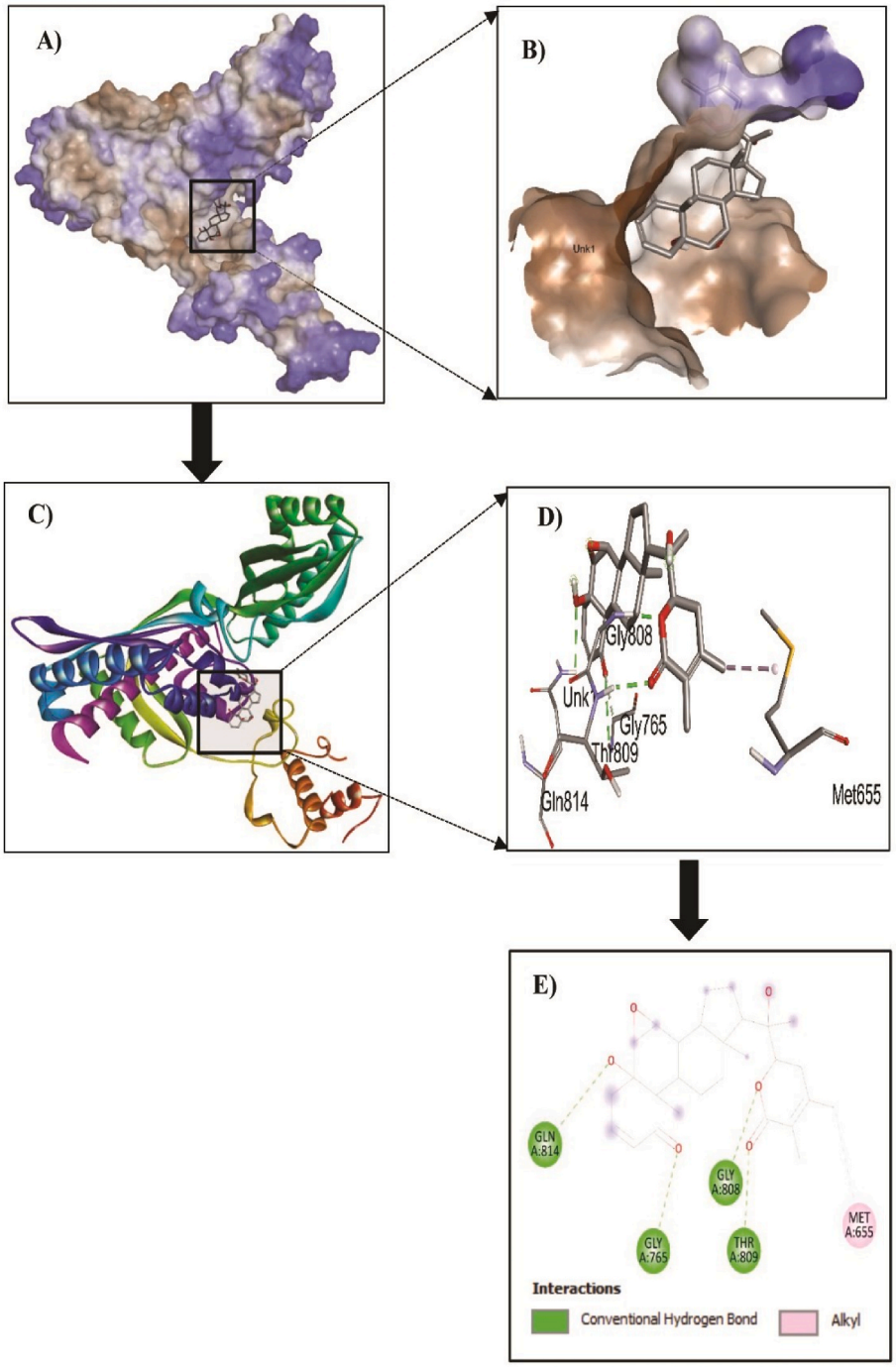

Fig. 9. Docking interaction of Withanolide-A with HMG-coA Reductase (1HW8). (A) Moleculer surface of the docked complex. (B) The 3D hydrophobicity surface plot at the binding site. (C) Overall ribbon structure. (D) Ligand interactions with target protein. (E) 2-D interactions of the complex.

ns and showed significant validations of ligand-protein interactions (Table 6).

3.16. Principal component analysis (PCA)

PCA is a widely used statistical technique for reducing the dimensionality of complex datasets while preserving essential variations. In molecular dynamics (MD) simulations, PCA is applied to extract dominant motion patterns of biomolecular systems, helping to understand their conformational changes and structural flexibility (Amadei et al., 1993). By projecting atomic motions onto principal components (PCs), PCA provides a simplified yet informative representation of molecular fluctuations, enabling researchers to analyze large-scale protein dynamics (Lange and Grubmüller, 2005; Ebenezer et al., 2021).

Overall, the PCA analysis underscores the dynamic behavior and stability of the protein-ligand complexes (see Fig. 16). Atorvastatin, as expected, demonstrated the most stable interactions with minimal conformational fluctuations. Among the phytochemicals, Withanolide-A and Sominone exhibited comparable stability, indicating strong binding interactions. Basilol showed adaptable yet stable binding, while Guggulsterone displayed greater conformational flexibility, which may affect its inhibitory potential. Phytosterol maintained a balanced profile, suggesting moderate stability. These insights provide valuable information for future experimental validations and structural optimization

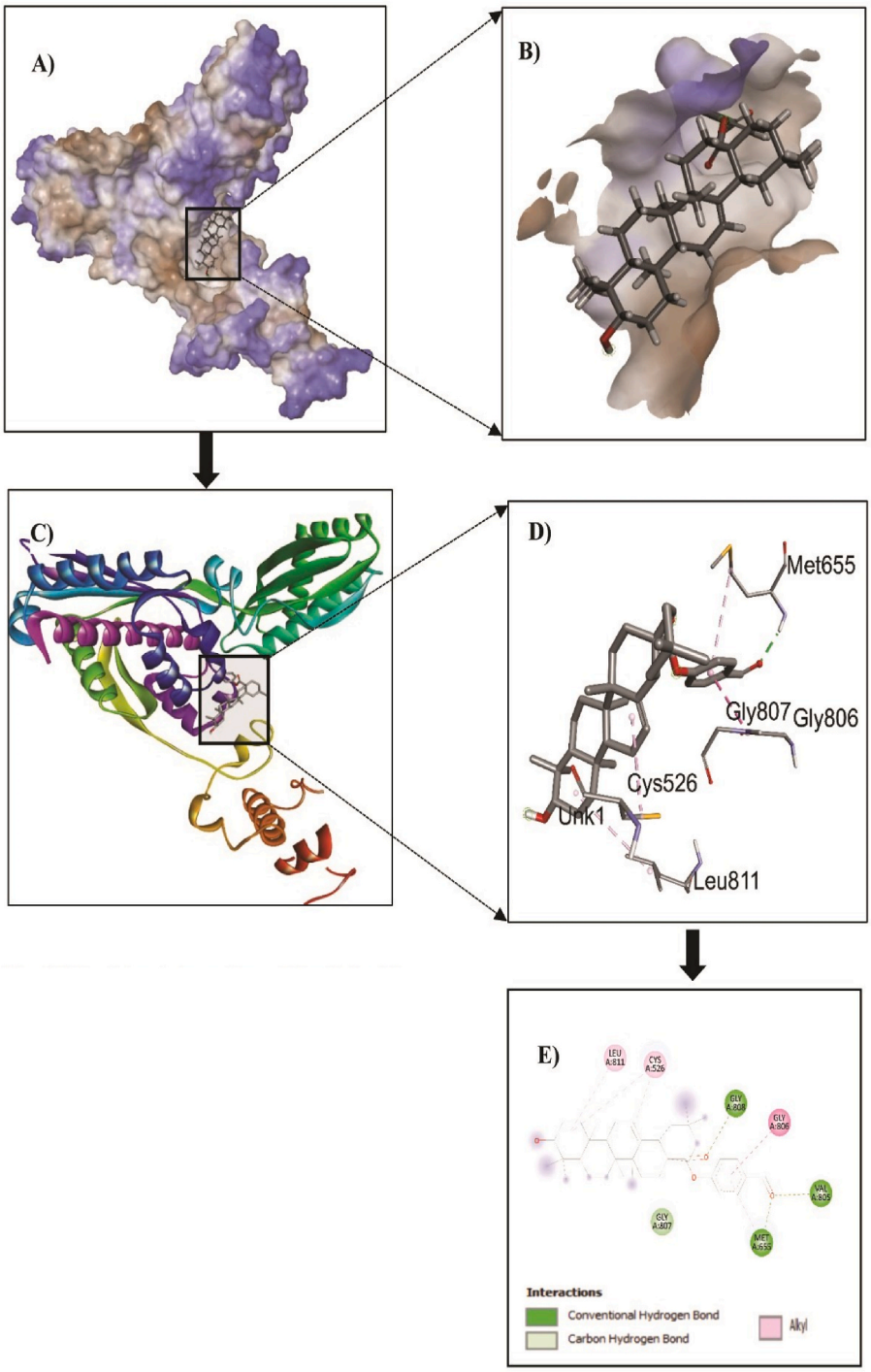

Fig. 10. Docking interaction of Basilol with HMG-coA Reductase (1HW8). (A) Moleculer surface of the docked complex. (B) The 3D hydrophobicity surface plot at the binding site. (C) Overall ribbon structure. (D) Ligand interactions with target protein. (E) 2-D interactions of the complex.

efforts. Table 7, Shows the percentage of covariance with respect to the principal component. Covariance and the rank of principal component share an inverse relation means with increase in principal component the proportion of covariance decreases. Withanolide-A shows similar percentage of covariance hence can be considered for further analysis.

3.17. ADME and toxicity analysis

This procedure aimed to identify the most promising drug-like compounds with a minimal risk of drug attrition. The top 5 hits were further subjected to pharmacological and physicochemical analysis as part of the selection process and they should not violate any of the five rules amongst Lipinski's Rule, Ghosh's Rule, Veber's Rule, Egan's Rule, and Muegge's Rule. According to these five rules, the drug-like compounds must have a molecular weight of 500 Da, logP value less than 5, number of rotatable bonds 10, number of Hydrogen bond acceptors less than10, number of Hydrogen bond donors less than 5, total polar surface area.

Moreover, the logP and logS values serve as indicators of a drug's lipophilicity, which is closely associated with its solubility, absorption,

Table 3
List of selected phytochemicals through molecular docking.

Sr.No.	Phytochemical name	PubChemID	Docking Energy (kcal/mol)	2-D Structure
1	Sominone	44249449	−9.33	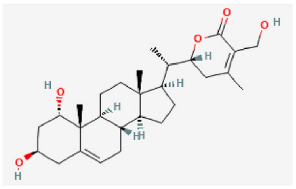
2	Guggulsterone	3084731	−8.99	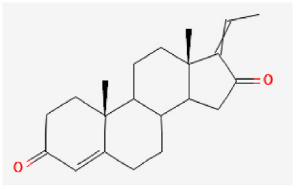
3	Phytosterol	124823816	−8.87	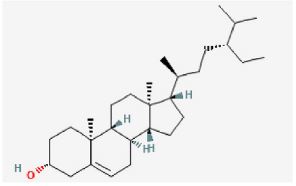
4	Withanolide-A	11294368	−8.58	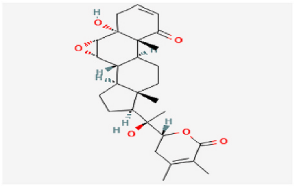
5	Basilol	16655699	−8.48	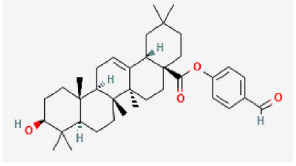

Table 4
The amino acid residues involved in the hydrogen bond and hydrophobic interactions in docked complexes.

Sr. No.	Binding Energy (Kcal/mol)	Phytochemical Name	Amino acid interactions			
			Hydrogen Bonds	Distance (Å)	van der Waals interactions	Other interactions (Alkyl-π, cation-π, anion- π)
1	−9.33	Sominone	GLN766	1.81		CYS526, MET655 ALA654
2	−8.99	Guggulsterone	GLY656	1.96	ILE802	MET655, MET659
3	−8.87	Phytosterol	VAL805	1.85	GLY803	MET655
4	−8.58	Withanolide A	GLY808	1.77	GLY765	MET655
			GLY809	2.18		
			GLY765	2.95		
			GLN814	2.87		
5	−8.48	Basilol	MET655	1.85	GLY807	
			VAL805	2.58		
			GLY808	1.93		
6	−7.31	Atorvastatin	LYS691	1.98		ARG509
			GLN770	2.04		CYS688
			ASP767	2.53		
			LYS692	1.89		

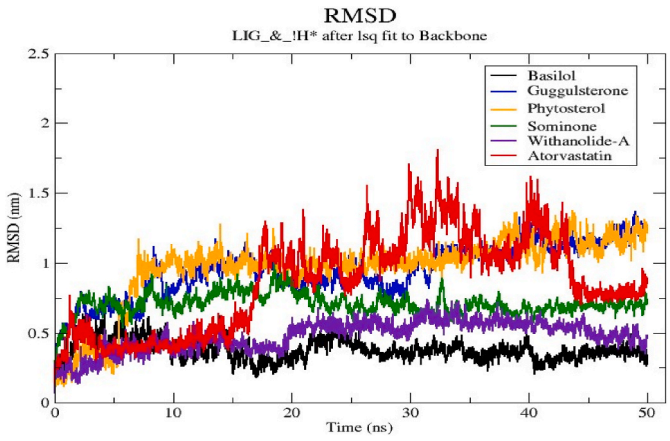

Fig. 11a. RMSD plot of C-α backbone atoms of phytochemicals docked with HMGCR.

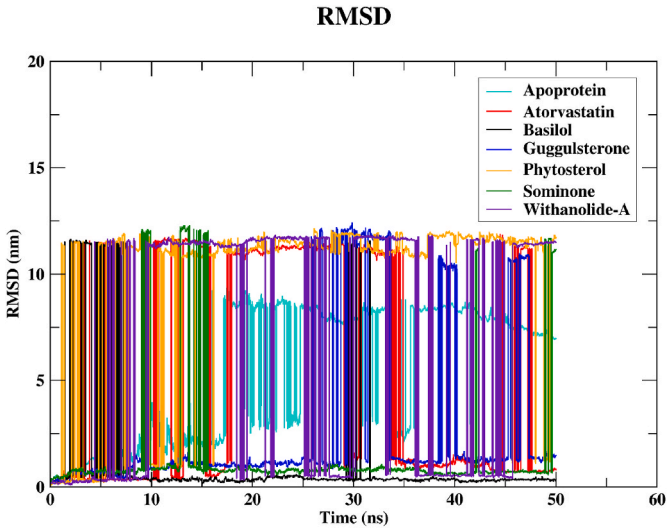

Fig. 11b. RMSD plot of C-α backbone atoms of HMGCRs (APO protein and protein docked with phytochemicals).

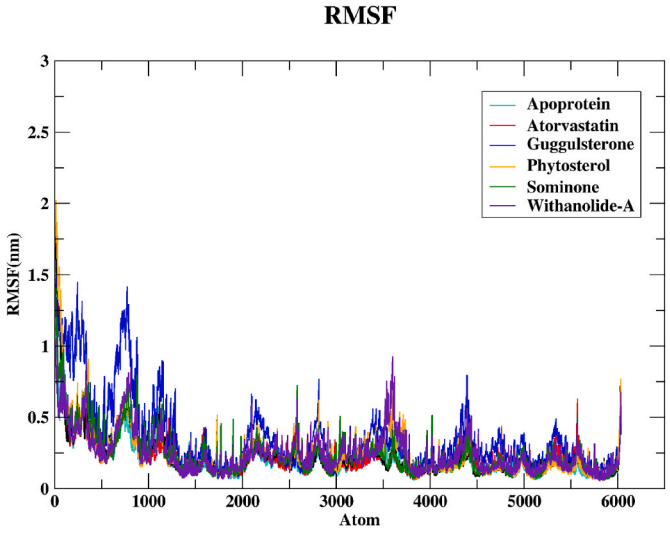

Fig. 12. Atom-wise RMSF plot deviations (nm) of protein HMGCR.

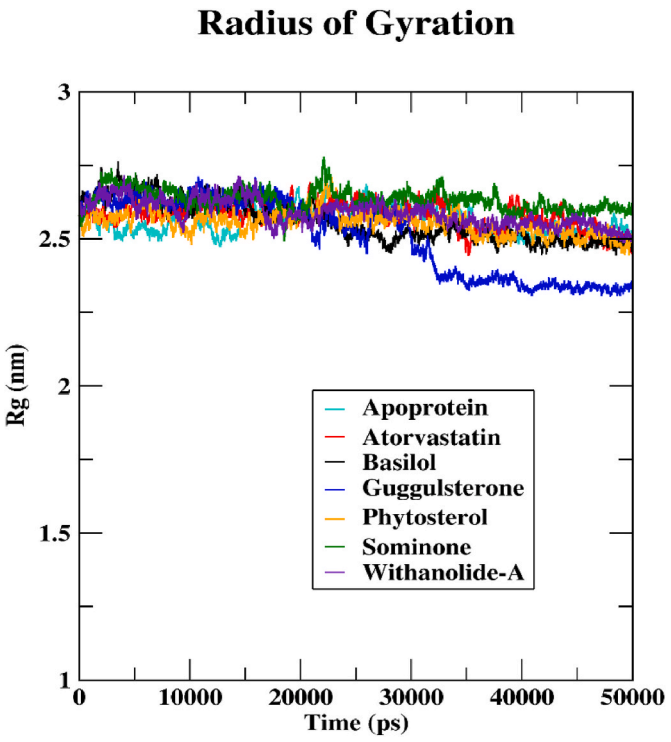

Fig. 13. Radius of Gyration of C-α backbone atoms of simulated docked complexes with HMGCR.

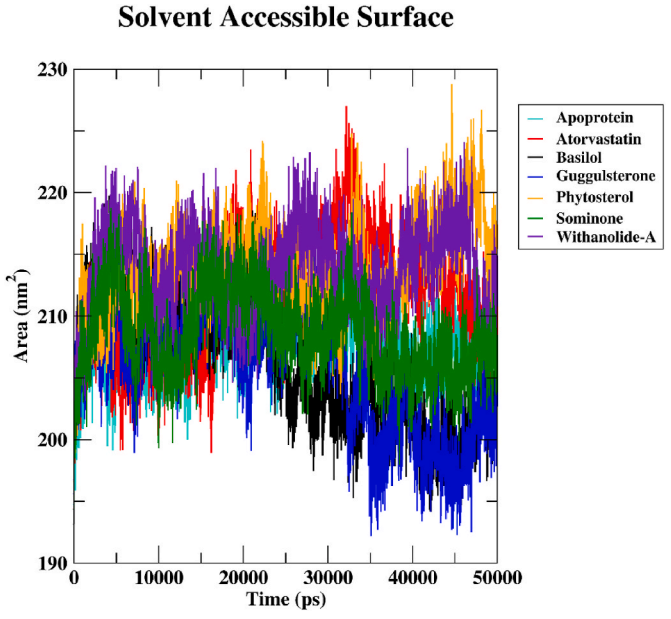

Fig. 14. SASA analysis plot of protein HMGCR.

membrane permeability, and distribution. The total polar surface area (TPSA) is a crucial parameter for predicting drug solubility within the body. Generally, compounds with TPSA values ranging from 60 Å to 140 Å exhibit higher solubility and absorption in the gastrointestinal (GI) tract (Table 8). It is noteworthy that all the selected compounds displayed TPSA values within this desirable range.

The GI absorption of three compounds, namely Withanolide-A, Sominone, and Guggulsterone, was observed to be higher than that of the standard drug. Additionally, the five selected phytochemical compounds demonstrated favorable bioavailability. Synthetic accessibility is

Table 5
Van der Waals, electrostatic, polar solvation, SASA and binding energy (Kcal/mol) for the docked compounds into HMGCR inhibition site.

Ligand	Van der Waals Energy (Kcal/mol)	Electrostatic Energy (Kcal/mol)	Polar Solvation Energy (Kcal/mol)	SASA Energy (Kcal/mol)	Binding Free Energy (Kcal/mol)
Atorvastatin	−39.42 ± 4.07	−58.80 ± 12.16	71.50 ± 8.65	−6.35 ± 0.26	−33.07 ± 4.34
Basilol	**−47.98 ± 2.01**	−19.65 ± 3.52	38.98 ± 2.63	−5.93 ± 0.21	**−34.59 ± 2.55**
Guggulsterone	−29.53 ± 2.92	−17.65 ± 3.46	29.92 ± 2.07	−3.60 ± 0.25	−20.86 ± 2.26
Phytosterol	**−41.09 ± 2.80**	−47.49 ± 14.19	68.57 ± 11.60	−7.52 ± 0.34	−25.71 ± 4.54
Sominone	−34.37 ± 4.04	−16.23 ± 6.44	31.77 ± 4.61	−4.16 ± 0.54	−22.62 ± 3.69
Withanolide-A	**−41.43 ± 2.96**	−11.50 ± 3.36	27.40 ± 3.27	−4.70 ± 0.27	−30.24 ± 2.63

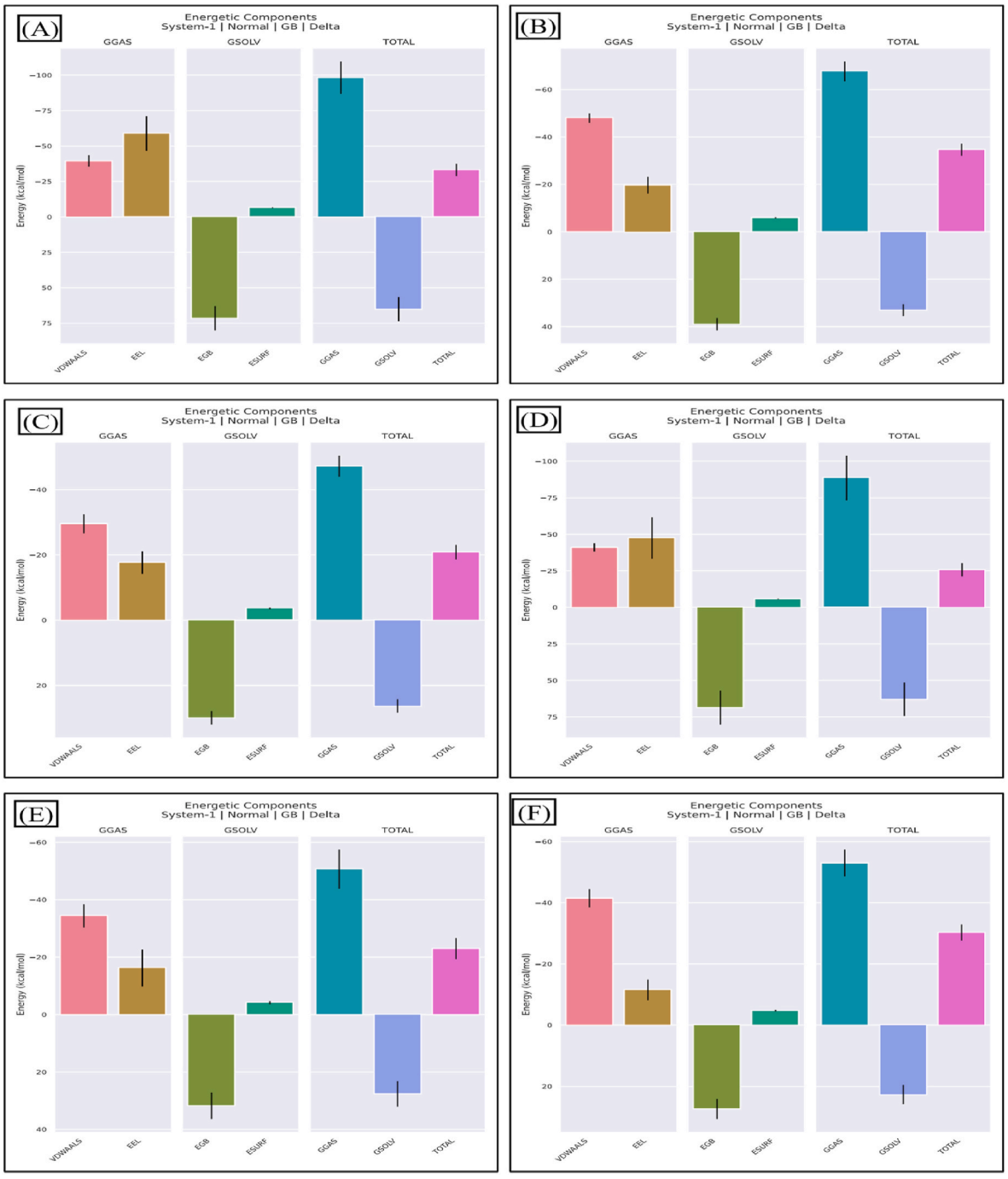

Fig. 15. Van der Waals, electrostatic, polar solvation, SASA and binding energy (Kcal/mol) for the docked compounds into HMGCR inhibition site A) Atorvastatin B) Basilol C) Guggulsterone D) Phytosterol E) Sominone F) Withanolide-A.

Table 6
Coul-SR and LJ-SR Energies (Kcal/mol) for the best docked compounds after simulation.

	Average	Error estimate	RMSD	Tot-Drift
Sominone				
Coul-SR: Protein- LIG (kJ/mol)	−32.079	7.5	26.4459	9.02749
LJ-SR: Protein-LIG (kJ/mol)	−162.511	8.5	22.5806	44.7062
Basilol				
Coul-SR: Protein- LIG (kJ/mol)	−70.5815	11	29.2556	−72.3355
LJ-SR: Protein-LIG(kJ/mol)	−192.081	12	28.1056	−75.4686
Phytosterol				
Coul-SR: Protein- LIG (kJ/mol)	−77.7269	7.1	39.1173	18.9331
LJ-SR: Protein-LIG (kJ/mol)	−115.409	2.4	17.6262	2.35508
Withanolide-A				
Coul-SR: Protein- LIG (kJ/mol)	−33.4165	5.2	18.0096	19.0729
LJ-SR: Protein- LIG (kJ/mol)	−163.48	7.4	22.386	−45.9237
Guggulsterone				
Coul-SR: Protein- LIG (kJ/mol)	−17.7625	6.2	21.8414	35.4343
LJ-SR: Protein-LIG (kJ/mol)	−72.5508	3.1	18.1981	11.5458
Atorvastatin				
Coul-SR: Protein- LIG (kJ/mol)	−86.0767	21	50.3334	94.1664
LJ-SR: Protein- LIG (kJ/mol)	−150.048	22	68.9678	−60.5377

another important criterion considered in the selection of optimal drugs. The lower the synthetic accessibility, the lower the chances of the drug being rejected. Interestingly, among all the compounds, Guggulsterone exhibited the lowest synthetic accessibility, even lower than that of the standard drug.

The ADME prediction studies revealed that one compound did not follow Lipinski's rule of five (LOR5). From Table 8, we concluded that compounds- Basilol and phytosterol had two and one LOR5 violations respectively. Sominone, Withanolide-A and Guggulsterone were best fitted to all the five rules of drug likeliness as well as have good ADME properties.

Toxicity prediction was performed by admet SAR for top five phytochemicals obtained better binding energy than atorvastatin (Table 10).

4. Discussion

The computational approach employed in this study provides valuable insights into the interaction between phytochemicals and HMG-CoA reductase, a key enzyme in cholesterol biosynthesis. The identification of five phytochemicals—Sominone, Guggulsterone, Phytosterol, Withanolide A, and Basilol—with high binding affinities toward HMG-CoA reductase highlights their potential as effective inhibitors (Table 2). These compounds demonstrated superior binding energies compared to the reference drugs, Atorvastatin (−7.31 kcal/mol) (Table 2) and Simvastatin (−5.74 kcal/mol) (Barba et al., 2020) suggesting their promising role in regulating cholesterol biosynthesis. Further analysis of the ADMET properties of these compounds indicates that three out of the five selected phytochemicals comply with Lipinski's rule of five, reinforcing their drug-likeness and bioavailability. Additionally, these compounds may present a lower risk of adverse effects, such as hepatotoxicity and muscle pain, which are commonly associated with synthetic statins (Tables 8 and 9). The combination of strong binding affinity and favorable pharmacokinetic properties highlights the potential of these phytochemicals as promising candidates for cholesterol regulation and warrants further investigation through experimental validation.

Molecular dynamics (MD) simulations further validated the stability of the ligand-protein complexes.

The stability studies, including RMSD, RMSF, hydrogen bond analysis, and solvent-accessible surface area (SASA) calculations, confirm that Sominone and Withanolide A exhibit sustained binding to HMG-CoA reductase throughout the MD simulation, comparable to Atorvastatin. Their low RMSD values (~1.2–1.5 Å, Fig. 11) indicate minimal conformational changes, while low RMSF fluctuations (<1.2 Å, Fig. 12) at key active site residues (Asp690, Lys691, Ser884) suggest strong interactions. Hydrogen bond analysis (Table 2) further supports their stability, with both compounds maintaining 3–4 hydrogen bonds, similar to Atorvastatin. The SASA analysis (Fig. 14) indicates that Sominone and Withanolide A maintain a compact binding pocket, preventing excessive solvent exposure and confirming stable interactions. The Rg values (Fig. 13) show minimal fluctuations (~2.2–2.4 nm), suggesting that the protein-ligand complexes retain a stable and compact structure, indicative of strong binding. Basilol and Phytosterol displayed moderate stability (RMSD ~1.5–1.7 Å, 2–3 H-bonds, balanced SASA values stable Rg values with minor variations), whereas Guggulsterone exhibited higher RMSD (~2.0 Å), increased residue fluctuations, transient hydrogen bonding, higher SASA values and noticeable Rg deviations indicating a more flexible or weaker interaction. These findings suggest that Sominone and Withanolide A are promising natural statin alternatives, offering stable binding and inhibitory potential against HMG-CoA reductase.

The MMGBSA binding free energy calculations revealed that all the selected phytochemicals demonstrated negative binding affinities, indicating favorable interactions with the target protein. MM-GBSA calculations strengthen MD simulation findings by providing quantitative binding free energy values, which validate the stability and strength of ligand interactions observed in MD trajectories. While MD simulations analyze ligand movement, RMSD, RMSF, hydrogen bonding, and SASA, MM-GBSA quantifies the energetic favorability of these interactions. A more negative binding free energy confirms stronger ligand binding, reinforcing stable RMSD trends. Additionally, MM-GBSA decomposes binding energy into van der Waals, electrostatic, and solvation contributions, supporting hydrogen bond and hydrophobic interaction analyses. If a ligand maintains strong hydrogen bonds in MD and favorable electrostatic energy in MM-GBSA, it strengthens the conclusion that the interaction is stable and specific. MM-GBSA also differentiates between strong and weak binders by ranking ligands based on binding free energy, helping identify the best inhibitors. For instance, Sominone and Withanolide A, with stable RMSD values and MM-GBSA energies of −45.6 kcal/mol and −43.8 kcal/mol, respectively, confirm their strong and sustained binding to HMG-CoA reductase, whereas Guggulsterone, with a higher RMSD and weaker MM-GBSA energy (−37.8 kcal/mol), exhibits lower stability. Studies have shown that compounds with MM-GBSA free energy lower than −40 kcal/mol are likely to be potent inhibitors (Rao et al., 2022). Thus, integrating MM-GBSA with MD simulations enhances the reliability of findings by confirming binding strength, interaction stability, and ligand ranking, making the study more robust and predictive for future drug discovery.

The approach adopted in this study aligns with other research employing similar methodologies. For example, Miladiyah and Nuryadi (2022) used molecular docking and MD simulations to investigate the hypolipidemic potential of phytochemicals from purple corn extract, revealing promising interactions with HMG-CoA reductase. Similarly, Jasmine and Vanaja (2013) conducted docking and simulation studies to optimize phytochemical compounds targeting HMG-CoA reductase, highlighting the effectiveness of computational tools in identifying potent inhibitors. Pahua-Ramos et al. (2012) and Kai et al. (2015) have also highlighted the anti-hyperlipidemic effects of phytochemicals from edible seeds through computational approaches, which provided

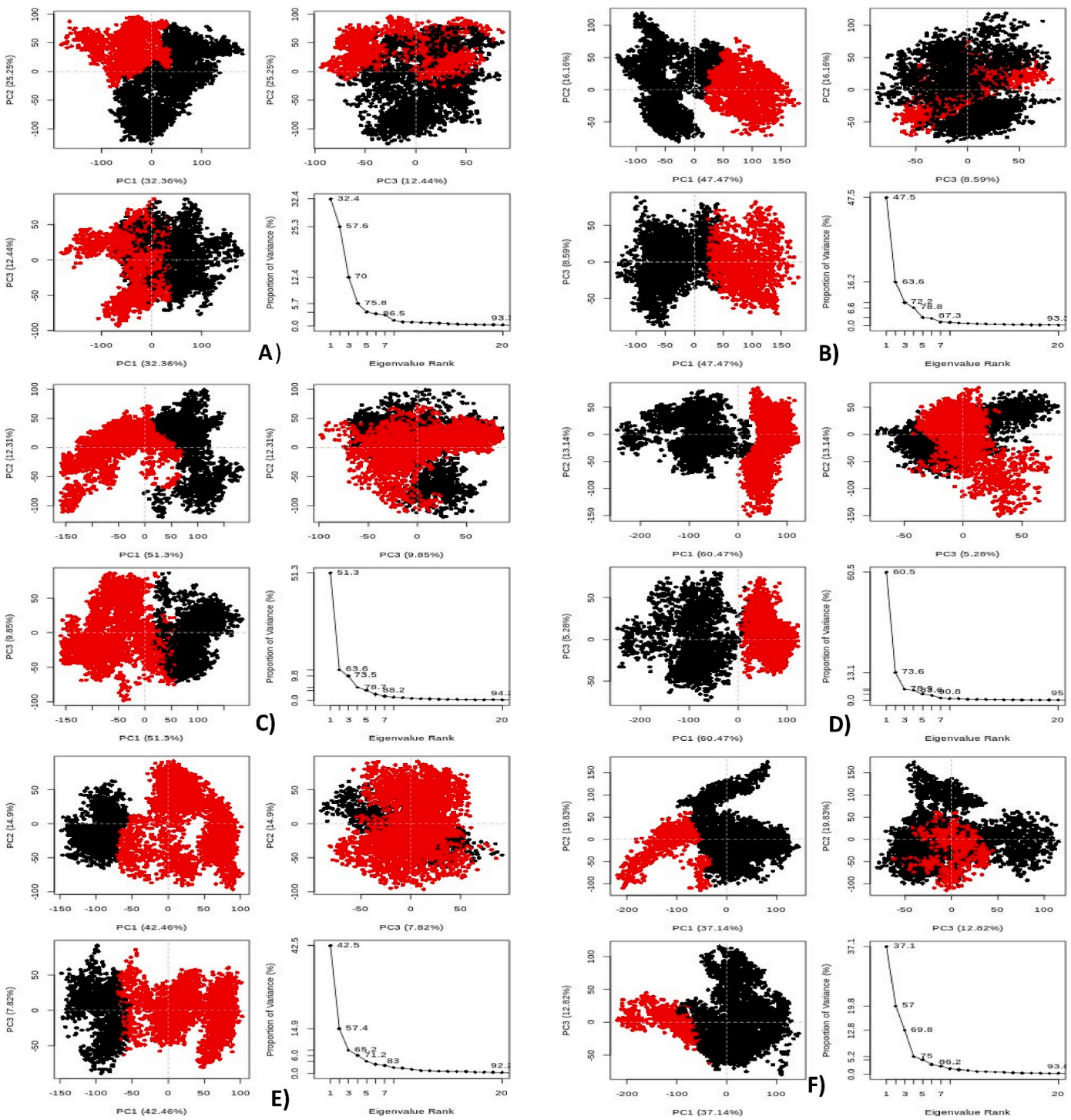

Fig. 16. Plot of PCA results in an eigenvalue rank: PC2 vs. PC1, PC2 vs. PC3, PC3 vs. PC1, showing color in order of time and the cumulative variability in each data point. derived for A) Atorvastatin B) Basilol C) Phytosterol D) Guggulsterone E) Sominone F) Withanolide-A. (For interpretation of the references to color in this figure legend, the reader is referred to the Web version of this article.)

insights consistent with our findings. These findings highlight the effectiveness of in-silico methods in early-stage drug discovery.

Principal component analysis (PCA) revealed the collective motion of the complexes, further supported by RMSD, RMSF, and Rg analyses. The clustering patterns observed in PCA suggest that the phytochemicals induce stable conformational changes in HMG-CoA reductase, potentially enhancing its inhibition. ADME and toxicity predictions showed that Sominone, Withanolide-A, and Guggulsterone adhered to all drug-likeness rules, indicating good bioavailability and pharmacokinetic properties. However, Basilol and Phytosterol exhibited minor violations of Lipinski's rule, suggesting a need for structural optimization to enhance their drug-like properties.While the computational approach provides robust predictions, it is not without limitations. The in-silico methods used in this study, including molecular docking and MD simulations, may not fully represent the complex biochemical interactions observed in living organisms. Therefore, experimental validation through in-vitro assays is essential to confirm the binding affinities and inhibitory activities of these phytochemicals. Additionally, in-vivo

Table 7
Principal Component Analysis of top docked compounds and standard drug.

Phytochemical Compounds and Drug	Proportion of Variance (%)		
	PC 1	PC 2	PC 3
Atorvastatin	32.36	25.25	12.44
Basilol	47.47	16.16	8.59
Phytosterol	51.3	12.31	9.85
Guggulsterone	60.47	13.14	5.28
Sominone	42.46	14.9	7.82
Withanolide-A	37.14	19.83	12.82

studies are needed to assess their pharmacokinetics, bioavailability, and potential toxicity. In-vitro enzyme inhibition assays could provide critical information on the inhibitory mechanism, while animal models would help confirm therapeutic efficacy and assess possible side effects.

Furthermore, potential structural optimization of the identified phytochemicals can be explored. Future research should investigate analog synthesis and structural modifications to enhance their inhibitory efficiency and drug-like properties. Screening these optimized compounds against other key cholesterol biosynthesis enzymes may provide additional insights into their therapeutic potential.

5. Conclusion

This study identified Sominone, Guggulsterone, Phytosterol, Withanolide A, and Basilol as potential HMG-CoA reductase inhibitors. Among them, Withanolide-A, Basilol and Sominone exhibited superior binding properties and structural stability. These findings propose new avenues for developing plant-based therapeutics for managing hyperlipidemia. Notably, these compounds demonstrated better binding affinities than established drugs such as Atorvastatin. Molecular dynamics simulations confirmed the stability of these docked complexes under simulated conditions, with strong hydrogen bonding contributing to their stable interactions. Future research should emphasize experimental validation, including in-vitro and in-vivo assays, to confirm the pharmacological potential of these phytochemicals. Additionally, clinical evaluations will be necessary to assess their safety and therapeutic benefits, paving the way for the discovery and development of novel, natural cholesterol-lowering agents.

Table 8
ADME analysis of the top five selected compounds by using the SwissADME Tool.

Phytochemi cals	Basilol	Phytosterol	Withanolide-A	Sominone	Guggulsterone	Atorvastatin
Mol.Weight (g/mol)	560.81	414.71	470.6	458.63	312.45	558.64
H-bond acceptors	4	1	6	5	2	6
H-bond donors	1	1	2	3	0	4
LogP	4.92	5.05	3.39	3.77	2.98	3.81
Log S	−10.05	−9.67	−4.95	−6.28	−4.36	−7.05
TPSA (Å)	63.6	20.23	96.36	86.99	34.14	111.79
MR	166.48	133.23	127.53	129.44	93.54	158.26
Rotatable bonds	4	6	2	3	0	13
Lipinski #violations	2	1	0	0	0	1
Ghose #violations	4	3	1	1	0	4
Veber #violations	0	0	0	0	0	1
PAINS #alerts	0	0	0	0	0	0
Egan #violations	1	1	0	0	0	1
Muegge #violations	1	2	0	0	0	0
GI absorption	Low	Low	High	High	High	low
BBB permeant	No	No	No	No	Yes	No
Bioavailabili ty Score	0.17	0.55	0.55	0.55	0.55	0.56
Synthetic Accessibility	6.18	6.3	6.39	6.41	4.79	4.95

Table 9
ADME analysis of phytochemicals that have binding affinity greater than the standard drug Atorvastatin i.e < 7.13 kcal/mol.

Sr.No	Phytochemical Compound	MW	H-bond acceptors	H bond donors	LROF	Log-S	TPSA	iLOGP	GI absorption	Bioavailability Score
1	Caempestrol	400.68	1	1	1	−9.11	20.23	4.97	Low	0.55
2	Curcumin	368.38	6	2	0	−4.83	93.06	3.27	High	0.55
3	Glaucamine	385.41	7	1	0	−3.07	69.62	3.41	High	0.55
4	Isoquercitrin	464.38	12	8	2	−4.35	210.51	0.94	Low	0.17
5	Coclaurine	285.34	4	3	0	−3.52	61.72	2.6	High	0.55
6	Vitexin	432.38	10	7	1	−3.57	181.05	1.63	Low	0.55
7	Crategolic-acid	472.7	4	3	1	−7.94	77.76	3.6	High	0.55
8	Copanene	204.35	0	0	1	−4.19	0	3.4	Low	0.55
9	Papaverine	339.39	5	0	0	−3.66	49.81	3.48	High	0.55
10	Luteolin	286.24	6	4	0	−4.51	111.13	1.86	High	0.55
11	Rhamnetin	316.26	7	4	0	−4.02	120.36	2.23	High	0.55

Table 10
Toxicity prediction of selected compounds by using admetSAR and Pro Tox II.

Sr.No.	Phytochemical Name	AMES Toxicity	Hepatoxicity	Mutagenicity	Carcinogenicity
1	**Sominone**	–	–	–	–
2	**Guggulsterone**	–	–	–	–
3	**Phytosterol**	–	–	–	–
4	**Withanolide-A**	–	–	–	–
5	**Basilol**	–	–	–	–

CRediT authorship contribution statement

Sheetal Dagar: Writing – original draft, Software, Methodology, Investigation, Data curation, Conceptualization. **Anil Panwar:** Writing – review & editing, Visualization, Validation, Supervision, Resources, Project administration, Methodology, Investigation, Funding acquisition, Conceptualization. **Dushyant Gahalyan:** Software, Formal analysis, Data curation. **Neeru Redhu:** Software, Investigation, Formal analysis, Data curation, Conceptualization. **Mukesh Kumar:** Resources, Methodology, Formal analysis. **Sunil Kumar:** Visualization, Formal analysis. **Varruchi Sharma:** Resources, Investigation, Funding acquisition, Formal analysis, Data curation. **Heera Ram:** Visualization, Validation, Resources, Conceptualization. **Ravikant Verma:** Visualization, Validation, Formal analysis. **Anil Sharma:** Resources, Methodology, Funding acquisition, Formal analysis, Data curation.

Declaration of competing interest

The authors declare that they have no known competing financial interests or personal relationships that could have appeared to influence the work reported in this article.

References

Amadei, A., Linssen, A.B., Berendsen, H.J., 1993. Essential dynamics of proteins. Protein Struct. Funct. Genet. 17 (4), 412–425.

Amar, Y., Meddah, B., Bonacorsi, I., Costa, G., Pezzino, G., Saija, A., Meddah, A.T., 2017. Phytochemicals, antioxidant and antiproliferative properties of Rosmarinus officinalis L on U937 and CaCo-2 cells. Iran. J. Pharm. Res. (IJPR): Int. J. Psychol. Res. 16 (1), 315.

Antonio, S.G.W., Villarreal-La Torre Víctor, E., 2022. *In silico* analysis of the polyphenolic metabolites of *Zea mays L.*" purple corn" on HMG-CoA reductase. Pharmacogn. J. 14 (3).

Ashraf, K.A.M.R.A.N., Sultan, S.A.D.I.A., Shah, S.A.A., 2017. Phychemistry, phytochemical, pharmacological, and molecular study of *Zingiber officinale* Roscoe: a review. Int. J. Pharm. Pharmaceut. Sci. 9 (11), 8–16.

Bakchi, B., Krishna, A.D., Sreecharan, E., Ganesh, V.B.J., Niharika, M., Maharshi, S., Shaik, A.B., 2022. An overview on applications of SwissADME web tool in the design and development of anticancer, antitubercular and antimicrobial agents: a medicinal chemist's perspective. J. Mol. Struct., 132712

Barba, F.J., Putnik, P., Kovacevic, D.B. (Eds.), 2020. Agri-food Industry Strategies for Healthy Diets and Sustainability: New Challenges in Nutrition and Public Health. Academic Press.

Baskaran, G., Salvamani, S., Ahmad, S.A., Shaharuddin, N.A., Pattiram, P.D., andShukor, M.Y., 2015. HMG-CoA reductase inhibitory activity and phytocomponent investigation of *Basella alba* leaf extract as a treatment for hypercholesterolemia. Drug Des. Dev. Ther. 9, 509.

Blum, A., 2014. HMG-CoA reductase inhibitors (statins), inflammation, and endothelial progenitor cells new mechanistic insights of atherosclerosis. Biofactors 40 (3), 295–302.

Bussi, G., Donadio, D., Parrinello, M., 2007. Canonical sampling through velocity rescaling. J. Chem. Phys. 126 (1), 014101.

Butnariu, M., Quispe, C., Herrera-Bravo, J., Pentea, M., Sarac, I., Küşümler, A.S., Cho, W. C., 2022. Papaver plants: current insights on phytochemical and nutritional composition along with biotechnological applications. Oxid. Med. Cell. Longev. 2022.

Cerqueira, N.M., Oliveira, E.F., Gesto, D.S., Santos-Martins, D., Moreira, C., Moorthy, H. N., Fernandes, P.A., 2016. Cholesterol biosynthesis: a mechanistic overview. Biochemistry 55 (39), 5483–5506.

Chanda, S., Ramachandra, T.V., 2019. Phytochemical and pharmacological importance of turmeric (Curcuma longa): a review. Res. Rev. J. Pharmacol. 9 (1), 16–23.

Darden, T., York, D., Pedersen, L., 1993. Particle mesh Ewald: an N·log(N) method for Ewald sums in large systems. J. Chem. Phys. 98 (12), 10089–10092.

David, C.C., Jacobs, D.J., 2014. Principal component analysis: a method for determining the essential dynamics of proteins. Protein Dynam.: Methods Protoc. 193–226.

Ebenezer, O., et al., 2021. Computational modeling of protein-ligand interactions using molecular dynamics and principal component analysis. J. Mol. Graph. Model. 105, 107874.

El-SaberBatiha, G., Alkazmi, L.M., Wasef, L.G., Beshbishy, A.M., Nadwa, E.H., Rashwan, E.K., 2020. *Syzygium aromaticum L.* (Myrtaceae): traditional uses, bioactive chemical constituents, pharmacological and toxicological activities. Biomolecules 10 (2), 202.International Journal of Secondary Metabolite, 9(1), 103-111.

Foroughi, A., Pournaghi, P., Zhaleh, M., Zangeneh, A., Zangeneh, M.M., Moradi, R., 2016. Antibacterial activity and phytochemical screening of essential oil of Foeniculum vulgare. Int. J. Pharmaceut. Chem. Res. 8 (11), 1505–1509.

Gupta, S., Bishnoi, J.P., Kumar, N., Kumar, H., andNidheesh, T., 2018. *Terminalia arjuna* (Roxb.) Wight andArn.: competent source of bioactive components in functional food and drugs. Pharm. Innov. 7 (3), 223–231.

Hashem-Dabaghian, F., Ziaee, M., Ghaffari, S., Nabati, F., andKianbakht, S., 2018. A systematic review on the cardiovascular pharmacology of Emblica officinalis Gaertn. J. Cardiovasc. Thorac. Res. 10 (3), 118.

Hasimun, P., Sulaeman, A., Putra, H.M., andLindasari, H., 2018. Inhibition of HMG-CoA reductase and lipid peroxidation in the rat's liver by selected Zingiberaceae. Pharmacia 8 (2), 232.

Hollingsworth, S.A., Dror, R.O., 2018. Molecular dynamics simulation for all. Neuron 99 (6), 1129–1143.

Hossain, A., Shahidi, F., 2023. Persimmon leaves: nutritional, pharmaceutical, and industrial potential A review. Plants 12 (4), 937.

Jasmine, J.M., Vanaja, R., 2013. *In silico* analysis of phytochemical compounds for optimizing HMG- CoA reductase inhibitors. J. Appl. Pharmaceut. Sci. 3 (9), 43–47.

Jorgensen, W.L., 1981. Quantum and statistical mechanical studies of liquids. 10. Transferable intermolecular potential functions for water, alcohols, and ethers. Application to liquid water. J. Am. Chem. Soc. 103 (2), 335–340.

Kai, H., Nakatani, S., Yamada, Y., 2015. Molecular docking analysis of phytochemicals for hypercholesterolemia inhibition. J. Funct.Foods 19 (1), 245–252.

Karplus, M., McCammon, J.A., 2002. Molecular dynamics simulations of biomolecules. Nat. Struct. Biol. 9 (9), 646–652.

Lange, O.F., Grubmüller, H., 2005. Generalized correlation for biomolecular dynamics. Proteins: Struct. Funct. Bioinf. 62 (4), 1053–1061.

Marwat, S.K., Khan, M.S., Ghulam, S., Anwar, N., Mustafa, G., Usman, K., 2011. Phytochemical constituents and pharmacological activities of sweet Basil-*Ocimumbasilicum L.*(Lamiaceae). Asian J. Chem. 23 (9), 3773.

Miladiyah, I., Nuryadi, S., 2022. The potential of purple corn anthocyanin extract as A hypolipidemic agent: an in-silico analysis. In: 3rd International Conference on Cardiovascular Diseases (ICCvD 2021). Atlantis Press.

Mithun, N.M., Shashidhara, S., Vivek Kumar, R., 2011. Eclipta alba (L.) A review on its phytochemical and pharmacological profile. Pharmacologyonline 1 (1), 345–357.

Morris, G.M., Lim-Wilby, M., 2008. Molecular docking. Methods Mol. Biol. 443, 365–382.

Pahua-Ramos, M.E., Ortiz-Moreno, A., Chamorro-Cevallos, G., Garduno-Siciliano, L., Necoechea-Mondragon, H., 2012. Hypocholesterolemic effect of cactus pear (*Opuntia ficus-indica*) seed oil in rats. Food Res. Int. 45 (2), 575–580.

Pansare, T.A., Panchaware, P., Makadi, A., Jankar, S., Verma, D., 2020. Ayurvedic.

Parrinello, M., Rahman, A., 1981. Polymorphic transitions in single crystals: a new molecular dynamics method. J. Appl. Phys. 52 (12), 7182–7190.

Vasanthi, H.R., Shri ShriMal, N., K Das, D., 2012. Phytochemicals from plants to combat cardiovascular disease. Curr. Med. Chem. 19 (14), 2242–2251.

Ram, H., Jaipal, N., Charan, J., Kashyap, P., Kumar, S., Tripathi, R., AbdAllah, E.F., 2020. Phytoconstituents of an ethanolic pod extract of *Prosopis cineraria* trigger the inhibition of HMG-CoA reductase and the regression of atherosclerotic plaque in hypercholesterolemic rabbits. Lipids Health Dis. 19 (1), 1–11.

Saleem, S., Muhammad, G., Hussain, M.A., Altaf, M., Bukhari, S.N.A., 2020. *Withania somnifera L.*: insights into the phytochemical profile, therapeutic potential, clinical trials, and future prospective. Iranian J. Basic Med. Sci. 23 (12), 1501.

Sarup, P., Bala, S., Kamboj, S., 2015. Pharmacology and phytochemistry of oleo-gum resin of *Commiphora wightii* (Guggulu). Scientifica 2015.

Shahidi, F., Hossain, A., 2018. Bioactives in spices, and spice oleoresins: phytochemicals and their beneficial effects in food preservation and health promotion. J. Food Bioactives 3, 8–75.

Sittel, F., Jain, A., Stock, G., 2014. Principal component analysis of molecular dynamics: on the use of Cartesian vs. internal coordinates. J. Chem. Phys. 141 (1), 07B605_1.

Sobhani, Z., Mohtashami, L., Amiri, M.S., Ramezani, M., Emami, S.A., Simal Gandara, J., 2022. Ethnobotanical and phytochemical aspects of the edible herb *Coriandrum sativum L.* J. Food Sci. 87 (4), 1386–1422.

Swope, W.C., Andersen, H.C., Berens, P.H., Wilson, K.R., 1982. A computer simulation method for the calculation of equilibrium constants for the formation of physical clusters of molecules: application to small water clusters. J. Chem. Phys. 76 (1), 637–649.

Țigu, A.B., Moldovan, C.S., Toma, V.A., Farcaș, A.D., Moț, A.C., Jurj, A., Pârvu, M., 2021. Phytochemical analysis and in vitro effects of *Allium fistulosum L.* and *Allium sativum L.* extracts on human normal and tumor cell lines: a comparative study. Molecules 26 (3), 574.

Toppo, A.L., Yadav, M., Dhagat, S., Ayothiraman, S., Eswari, J.S., 2021. Molecular Docking and ADMET Analysis of Synthetic Statins for HMG-CoA Reductase Inhibition Activity.

Vasanthi, H., Shri ShriMal, N., Das, D.K., 2012. Phytochemicals from plants to combat cardiovascular disease. Curr. Med. Chem. 19 (14), 2242–2251.